



**THE EFFECTS OF GPS M-CODE
ON RADAR DETECTION**

THESIS

Jae K. Yang, Captain, USAF

AFIT/GE/ENG/03-20

**DEPARTMENT OF THE AIR FORCE
AIR UNIVERSITY**

AIR FORCE INSTITUTE OF TECHNOLOGY

Wright-Patterson Air Force Base, Ohio

APPROVED FOR PUBLIC RELEASE; DISTRIBUTION UNLIMITED

The views expressed in this thesis are those of the author and do not reflect the official policy or position of the United States Air Force, Department of Defense, or the United States Government.

AFIT/GE/ENG/03-20

THE EFFECTS OF GPS M-CODE ON RADAR DETECTION

THESIS

Presented to the Faculty of the
Department of Electrical and Computer Engineering
Graduate School of Engineering and Management
of the Air Force Institute of Technology
Air University
In Partial Fulfillment of the
Requirements for the Degree of
Master of Science

Jae K. Yang, BSEE, BSIE
Captain, United States Air Force

March, 2003

Approved for public release; distribution unlimited

THE EFFECTS OF GPS M-CODE ON RADAR DETECTION

Jae K. Yang, BSEE, BSIE

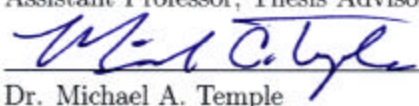
Captain, United States Air Force

Approved:



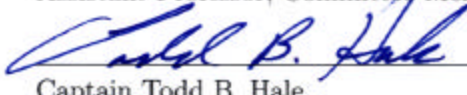
Major John F. Raquet
Assistant Professor, Thesis Advisor

14 MAR 03
Date



Dr. Michael A. Temple
Assistant Professor, Committee Member

14 Mar 03
Date



Captain Todd B. Hale
Assistant Professor, Committee Member

14 MAR 03
Date

Acknowledgements

There are several people that I would like to thank for their support and involvement with this thesis. First of all, I would like to thank my advisor, Maj John Raquet, who's patience and guidance cannot be captured with words. I am truly in debt to you. In addition, I would like to thank my committee members, Dr. Michael Temple and Capt Todd Hale. I would also like to thank my fellow GNC mates for making this a worthwhile experience because jobs come and go, but friendships last a lifetime. Last, and most importantly, I would like to thank the two loves of my life, my wife and my daughter. To my wife, I thank you for your understanding, patience and support with which I couldn't have done without. To my daughter, you are my inspiration to get up everyday to try and make this world a safer place for you to live, learn, and grow.

Jae K. Yang

Table of Contents

| | Page |
|--|------|
| Acknowledgements | iii |
| List of Figures | vi |
| List of Tables | viii |
| Abstract | ix |
| I. Introduction | 1-1 |
| 1.1 Background | 1-1 |
| 1.1.1 Current Signal Structure | 1-3 |
| 1.1.2 Modernized Signal Structure | 1-3 |
| 1.2 Problem Statement | 1-4 |
| 1.3 Summary of Current Knowledge | 1-4 |
| 1.4 Scope | 1-5 |
| 1.5 Thesis Organization | 1-5 |
| II. GPS Signal Structure and Radar Theory | 2-1 |
| 2.1 Overview | 2-1 |
| 2.2 GPS M-code | 2-1 |
| 2.3 Radar Theory | 2-4 |
| 2.3.1 Radar Pulse | 2-5 |
| 2.3.2 Radar Equation | 2-7 |
| 2.3.3 Target Detection | 2-10 |
| 2.4 Summary | 2-17 |

| | Page |
|---|-------|
| III. Simulation Methodology, Results, and Analysis | 3-1 |
| 3.1 Overview | 3-1 |
| 3.2 Simulation Description | 3-1 |
| 3.3 Simulation Process | 3-4 |
| 3.3.1 Baseline Case | 3-5 |
| 3.3.2 Signal Plus Noise Plus M-code Case | 3-12 |
| 3.4 Summary | 3-22 |
| IV. Conclusion and Recommendations | 4-1 |
| 4.1 Conclusion | 4-1 |
| 4.2 Recommendations | 4-2 |
| Bibliography | BIB-1 |

List of Figures

| Figure | | Page |
|--------|---|------|
| 1.1. | Received M-Code Power in Relation to the Noise Floor | 1-2 |
| 1.2. | Modernized GPS Signal Architecture | 1-4 |
| 2.1. | Example of the M-code PN Sequence | 2-2 |
| 2.2. | PSD of BOC(10,5) M-Code Modulation | 2-3 |
| 2.3. | PSD Comparison of C/A, P(Y), and M-code | 2-4 |
| 2.4. | Illustration of the Basic Radar Principle | 2-5 |
| 2.5. | Illustration of Pulse Characteristics | 2-6 |
| 2.6. | Range Ambiguity Illustration | 2-7 |
| 2.7. | Antenna Gain Characteristics | 2-8 |
| 2.8. | Simple Detection Circuit | 2-10 |
| 2.9. | Detection Concept | 2-11 |
| 2.10. | PDF of Detected Noise and Signal Plus Noise | 2-16 |
| 3.1. | Simulation Scenario | 3-2 |
| 3.2. | Radar RF Frequency Chosen to Maximize Received M-code Sig- nal Power | 3-3 |
| 3.3. | Receiver Model | 3-5 |
| 3.4. | Simulation Flow Diagram | 3-6 |
| 3.5. | Baseline Simulation Block Diagram | 3-6 |
| 3.6. | 8 th -Order Chebyshev Filter Response | 3-8 |
| 3.7. | Threshold Determination Example | 3-9 |
| 3.8. | Probability of Detection Curve for a $P_{FA} = 0.01$ | 3-11 |
| 3.9. | M-code Interference Simulation | 3-12 |
| 3.10. | P_D versus $\text{SNR}_D/\text{SNR}_{IF}$ for $P_{FA} = 0.01$ | 3-14 |

| Figure | | Page |
|--------|---|------|
| 3.11. | Detection Curves for Varying Levels of Received M-code Power for $P_{FA} = 0.01$ | 3-16 |
| 3.12. | P_D vs Received M-code Power for $P_{FA} = 0.01$ | 3-17 |
| 3.13. | Effects of Phase Offsets on P_D for Received M-code Power of -160 dBW and $P_{FA} = 0.01$ | 3-18 |
| 3.14. | Effects of Phase Offsets on P_D for Received M-code Power of -150 dBW and $P_{FA} = 0.01$ | 3-18 |
| 3.15. | Effects of Phase Offsets on P_D for Received M-code Power of -140 dBW and $P_{FA} = 0.01$ | 3-19 |
| 3.16. | Effects of Phase Offsets on P_D for Received M-code Power of -130 dBW and $P_{FA} = 0.01$ | 3-19 |
| 3.17. | Effects of Phase Offsets on P_D for Maximum Specified Received M-code Power of -131 dBW and $P_{FA} = 0.01$ | 3-20 |
| 3.18. | P_D Comparison Using Different Random M-code Sequences for Received Power of -160 dBW | 3-21 |
| 3.19. | P_D Comparison Using Different Random M-code Sequences for Received Power of -131 dBW | 3-21 |

List of Tables

| Table | | Page |
|-------|---|------|
| 2.1. | Received RF M-code Signal Strength Minima and Maxima . | 2-4 |
| 3.1. | Operating Parameters for the ARSR-4 System | 3-4 |
| 3.2. | Baseline Simulation Operating Points for Analysis | 3-11 |

Abstract

The GPS system is undergoing a modernization effort which will add several new signals to be placed at the L1, L2, and L5 frequency bands. One of the signals to be placed on L2 is a new military code (M-code) which may be transmitted at a higher power level than current GPS signals. Other users of the L2 frequency band are concerned with the potential interference that may be caused by the increase in power of the GPS signal. One particular use of the 1215-1400 MHz frequency band is Air Traffic Control (ATC) radar applications.

This thesis models an ARSR-4 radar system as a single pulse radar and simulates the effects that the M-code signal has on a radar system's detection capability. Looking at a worst case radar detection scenario, where the M-code signal power incident on the radar would be at a maximum, the results indicate that for the minimum specified received M-code signal power, the effects are minimal. However, for the maximum specified M-code signal power, the effects are quite noticeable to the point where the M-code may prevent detection of a single pulse.

The results only apply to a worst-case scenario for a single pulse radar. Further modeling of the ARSR-4 system, to include pulse integration, would be necessary before a definitive conclusion can be drawn that the M-code will significantly affect radar system performance.

THE EFFECTS OF GPS M-CODE ON RADAR DETECTION

I. Introduction

In a letter dated 10 August 2001, the International Civil Aviation Organization (ICAO) raised the following issue to be addressed at the International Telecommunication Union (ITU) World Radiocommunication Conference (2003) (WRC-2003):

“...the need to secure the protection of distance measuring equipment (DME) and radar systems from interference from radio navigation satellite service (RNSS) in the frequency bands 960-1215 MHz and 1215-1400 MHz” [16]

The ICAO is concerned about the potential interference that may result from the GPS modernization effort. The current received GPS signal power is below the noise floor so that most systems receiving the GPS signal as interference may not be able to distinguish the actual signal from noise. However, the modernization plan calls for an increase in the received GPS power of some signals by levels 20 dB greater than the current signals [14]. The increase in power pushes the received GPS signal close to the noise floor, which may cause interference to systems operating near the GPS frequency. This concern is illustrated in Figure 1.1, which shows the proposed GPS military signal (M-code) at two received power levels in relation to the noise floor.

1.1 Background

The Global Positioning System (GPS) was designed in the early 1970s to provide military and civil users with position estimates using radio navigation (radio waves) from a constellation of satellites orbiting 20,000 km above the earth. Since then, the world has changed, but the GPS policies and regulations adopted by the

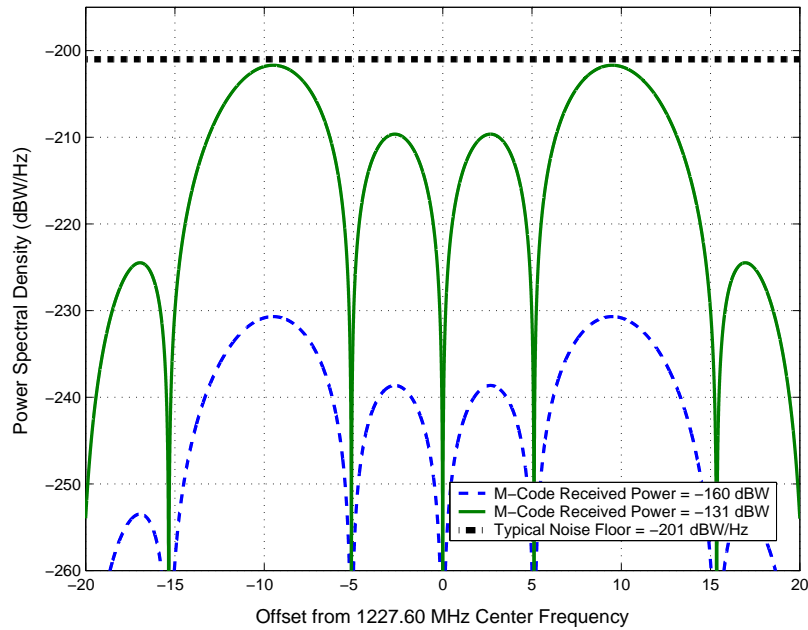


Figure 1.1 Received M-Code Power in Relation to the Noise Floor

U.S. Government for military and civilian users have generally remained constant. An increasing emphasis on commerce and the world's current political climate has given the civil users and GPS industry in the United States new influence to push for modifications in GPS design and policies. This emphasis became evident with the deactivation of Selective Availability (SA) in May 2000, which marked the first important change in U.S. policy [7].

The deactivation of SA was the result of the March 1996 Presidential Decision Directive (PDD) [3] which announced the “intention to discontinue the use of GPS Selective Availability (SA) within a decade”. The primary purpose of SA was to intentionally degrade GPS to reduce the capability of enemy forces using GPS. To replace the function of SA, the PDD also tasked the Department of Defense (DoD) “to develop measures to prevent the hostile use of GPS and its augmentations to ensure that the United States retains a military advantage without unduly disrupting or degrading civilian use.”

To comply with the directive, the GPS Joint Program Office (JPO) and the Space Warfare Center (SWC) conducted a study to identify the best GPS signal redesign to meet the needs of both the military and civilian GPS users for the next 30 years [2]. The results of that study were incorporated into what is now termed GPS Modernization.

1.1.1 Current Signal Structure. The current GPS signals reside on two L-band frequencies: L1 at 1575.42 MHz and L2 at 1227.6 MHz. The L1 frequency consists of two-spread-spectrum BiPhase Shift Keyed (BPSK) modulated signals in phase quadrature: the Precise (P)-code, with a 10.23 MHz chipping rate, and the Coarse/Acquisition (C/A)-code, with a 1.023 MHz chipping rate [2]. The P-code can be (and currently is) encrypted for anti-spoofing. When encrypted, the P-code is denoted P(Y)-code. The C/A-code is unencrypted and is used by military receivers for initial acquisition, while for civilian receivers it is the only navigation signal. The L2 frequency currently consists of only the P(Y)-code.

1.1.2 Modernized Signal Structure. The modernization plan calls for reusing the existing frequency bands. The L-band frequencies are especially well-suited for radionavigation from space and additional L-band spectrum for GPS is scarce. In addition, the technical limitations and the costs involved in modifying satellites to transmit at frequencies different from L1 and L2 are prohibitive [2]. Therefore, the modernized signal architecture will include the current signal structure with the addition of two new civil signals—one on L5 centered at 1176.45 MHz and another on L2 (L2C). In addition, a new military signal (M-code) will be placed on both L1 and L2. The resulting modernized GPS signal architecture is shown in Figure 1.2.

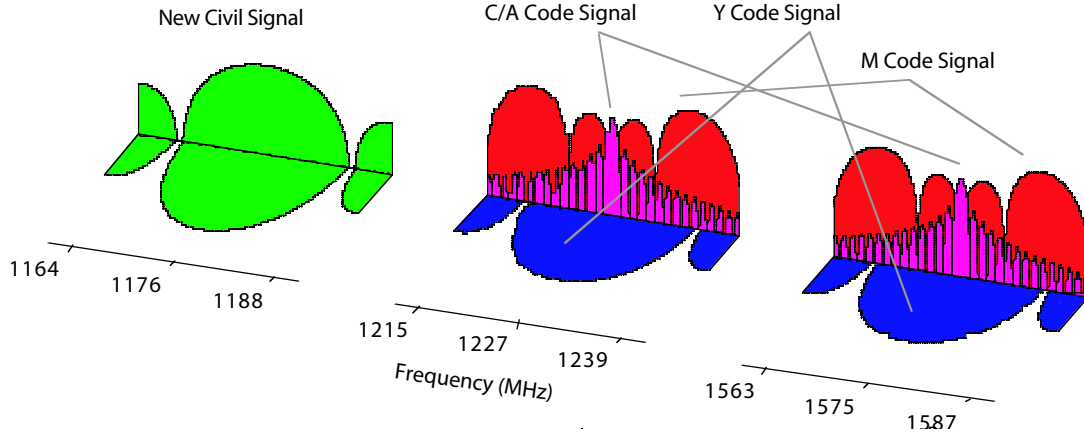


Figure 1.2 Modernized GPS Signal Architecture [4]

1.2 Problem Statement

Since GPS Modernization includes two new signals on the L2 band, other users of this frequency spectrum are concerned with the potential Radio Frequency Interference (RFI) that may be caused by the modernized GPS signals. To allay any concerns with the modernization plan, the interference issue must be addressed. Therefore, the objectives of this thesis are to model and simulate the effects of the modernized GPS signals on radar systems operating in the L2 band.

1.3 Summary of Current Knowledge

Numerous studies have examined the effects of RFI on GPS. Most conclude that GPS is vulnerable to both intentional (jamming) and unintentional interference sources. This vulnerability is a byproduct of the Direct Sequence Spread Spectrum (DS/SS) GPS signal structure and the long baseline between the satellites and receivers, which results in extremely low received power levels.

Very little attention has been paid to the effects of GPS interfering with other applications. As previously stated, the current GPS signal power is below the noise floor and most systems receiving the GPS signal as an interferer may not be able to distinguish the actual signal from noise. Furthermore, the National Telecommunications and Information Administration (NTIA) has stated that at the current GPS

signal power level, which has not changed since 1978, there have been no reports of harmful interference to other users in the frequency bands used by GPS [13]. However, with the increase in M-code power, this situation may no longer be the case.

The Federal Aviation Administration (FAA) recently conducted tests to determine what affect an increase in GPS satellite power would have on some of their radar systems. By varying the Interference-to-Noise (I/N) ratios from approximately -18 dB I/N to +21 dB I/N, the tests were designed to determine the impact on probability of detection, reduction in range, and the desensitizing of the radar [15]. As of Feb 2003, the final FAA test report has yet to be completed.

1.4 Scope

As discussed in Section 1.2, L2 is the primary frequency band of interest. Therefore, only the L2 band, transmitting the new civil signal (L2C), the legacy P(Y)-code and the new M-code, is considered for this effort. Furthermore, given that the current GPS signal power levels do not interfere with radar systems today, a majority of the analysis is focused on the M-code.

To bound the simulation, the radar system is modeled as a single pulse radar and the target is assumed stationary. The goal of the simulation is to determine the effects of the M-code on the radar system's ability to detect a target. In general, this research will involve a worst-case analysis of the effect of GPS M-code on an Air Traffic Control (ATC) radar.

1.5 Thesis Organization

Chapter 2 presents additional information on the GPS M-code signal and background information on radar theory. Chapter 3 presents the computer simulation model, simulation results and analysis. Finally, Chapter 4 summarizes the results of the thesis, discusses limitations, and provides recommendations for future research.

II. GPS Signal Structure and Radar Theory

2.1 Overview

This chapter presents detailed information on the military code (M-code) signal structure and a discussion on radar theory. The M-code discussion focuses on signal generation as compared with the C/A and P-codes, although, they will not be discussed in depth. The radar theory focuses on radar pulse characteristics, the range equation, and target detection. The M-code and radar theory information presented will be used for the simulation presented in Chapter 3. For a good review of the C/A and P-codes, the reader is directed to references [7] and [10].

2.2 GPS M-code

Understanding the M-code signal structure requires some insight into the GPS upgrade design goals. Some of these goals include [4]:

- Better jamming resistance than the current P(Y)-code signal accomplished through higher transmit power without causing C/A-code or P(Y)-code receiver interference.
- Compatibility with prevention jamming against enemy GPS use.
- More robust signal acquisition.
- Comparable, if not better, performance to the current P(Y)-code signal.
- Coexistence with current signals on L1 and L2, not interfering with current or future military user equipment.
- Simple and low-risk implementation on both space vehicles and in future user equipment - must be as power efficient as possible.

To achieve these goals, the M-code was designed to be modulated with a Binary Offset Carrier (BOC) signal having a subcarrier frequency of 10.23 MHz and

spreading code rate of 5.115 M spreading bits per second, denoted BOC(10.23,5.115) (abbreviated as BOC(10,5)). BOC modulation details are sufficiently covered in [5].

Mathematically the transmitted M-code signal can be written as [8]

$$S_M(t) = \sqrt{2P_M}d_M(t)SW(t)PN_5(t)\cos(\omega_{L1,2}t + \theta) \quad (2.1)$$

where

- P_M = Transmitted M-code power
- $d_M(t)$ = M-code data stream (25 or 100 bps)
- $SW(t)$ = 10.23 MHz Square wave carrier
- $PN_5(t)$ = 5.115 MHz Pseudo random code
- $\omega_{L1,2}$ = L1 or L2 angular frequency
- θ = Phase

Figure 2.1 shows an example of $SW(t)$, $PN_5(t)$, and the resultant baseband M-code sequence $SW(t)PN_5(t)$.

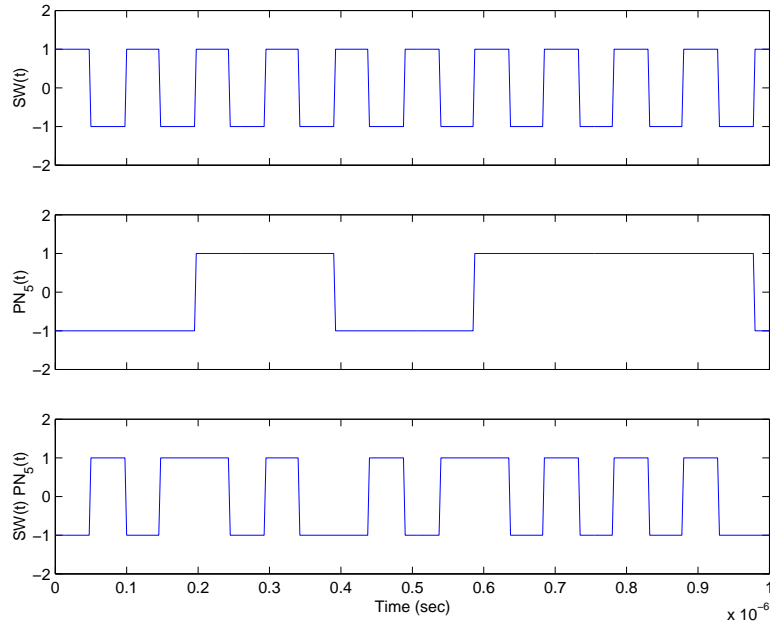


Figure 2.1 Example of the M-code PN Sequence

The main result of the BOC(10,5) modulation is that the majority of the power in the L2 frequency band is concentrated around offset frequencies. These frequencies are located 10.23 MHz above and below the carrier frequency as shown in Figure 2.2, where the power spectral density (PSD) is given by [14]

$$\text{PSD}_{\text{BOC}(f_s, f_c)}(f) = f_c \left(\frac{\sin\left(\frac{\pi f}{2f_s}\right) \sin\left(\frac{\pi f}{f_c}\right)}{\pi f \cos\left(\frac{\pi f}{2f_s}\right)} \right)^2 \quad (2.2)$$

where $f_s = 10.23 \times 10^6$ and $f_c = 5.115 \times 10^6$.

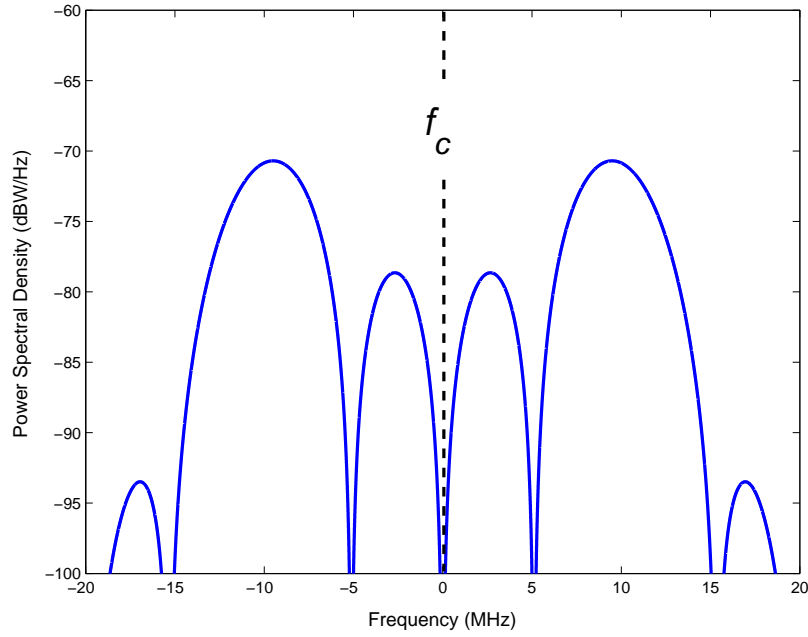


Figure 2.2 PSD of BOC(10,5) M-Code Modulation

Figure 2.3 illustrates a comparison of the M-code spectrum with that of the C/A and P(Y)-code signals, where all signals have 1 W power. From Figure 2.3, the M-code modulation's spectrum appears to be distinctly separated from that of the C/A and P(Y)-code signals. As a result, the M-code may be received at high power levels without degrading the performance of C/A and P(Y)-code receivers—a key design goal [6]. Table 2.1 shows the minimum and maximum user-received RF signal

power levels for the M-code, listed by satellite production version [14]. As stated previously, the effect of the potential increase in the maximum received RF power on ATC radar systems' detection capability is the primary focus of this thesis.

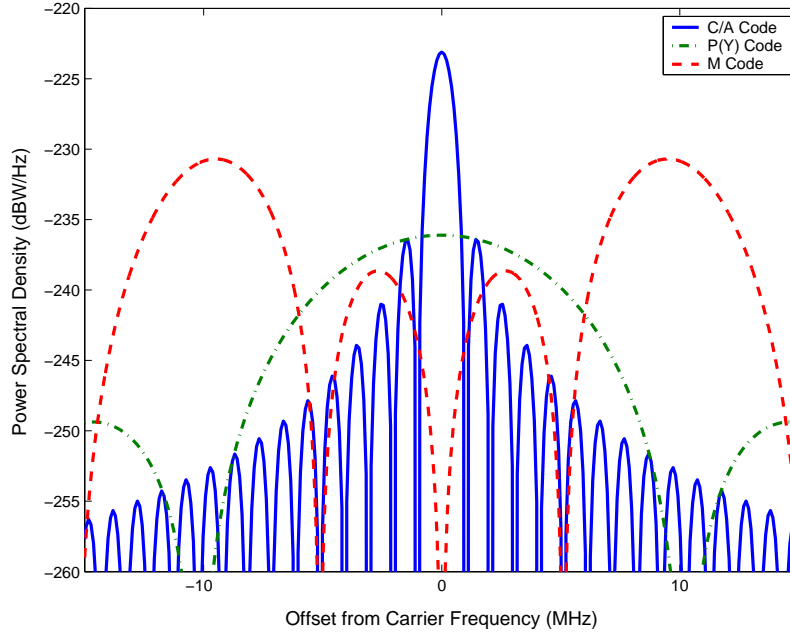


Figure 2.3 PSD Comparison of C/A, P(Y), and M-code

Table 2.1 Received RF M-code Signal Strength Minima and Maxima (dBW) [14]

| Production Version | Min | Max |
|--------------------|------|------|
| Block IIF | -160 | -153 |
| Block IIR-M | -160 | -153 |
| Future SVs | -158 | -131 |

2.3 Radar Theory

The term radar is an acronym for *R*Adio *D*etection And *R*anging [17]. Radars operate by radiating electromagnetic energy and examining the reflected energy for detection and range determination. The basic radar principle is illustrated in Figure 2.4.

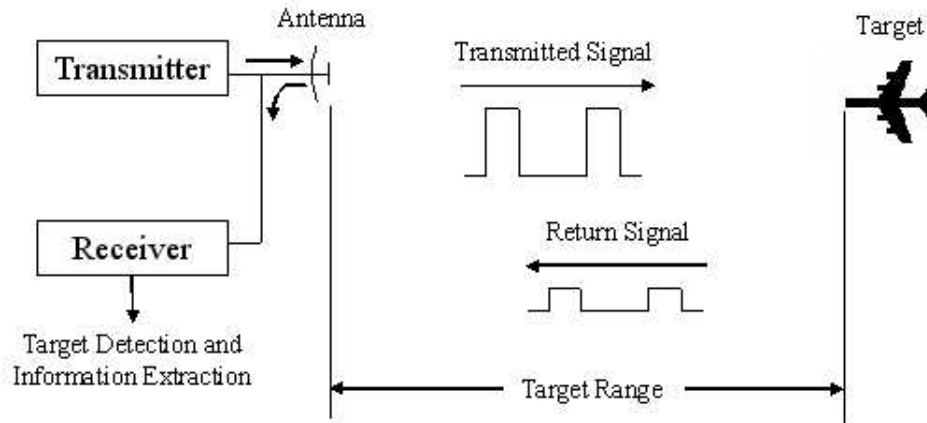


Figure 2.4 Illustration of the Basic Radar Principle

2.3.1 Radar Pulse. Most objects such as aircraft, ships, vehicles, buildings, or features of the terrain reflect radio waves, much as they do light. The only difference between radio waves and light are the transmission frequencies, where light is much higher. The reflected energy is scattered in many directions, but generally a detectable portion of it is scattered back to the original transmission point [18].

In most radar systems, the transmitter and receiver share a common antenna, as shown in Figure 2.4. In this configuration, the transmitter may interfere with the reception. To avoid this problem, the radio waves are generally transmitted in pulses, at which time the receiver is turned off.

The following terms are used to describe the pulse transmission as illustrated in Figure 2.5 [18]:

- Pulse Duration (τ) – Length of the transmitted pulse
- Interpulse Period (T) – The time between transmitted pulses
- Pulse Repetition Frequency (PRF) – Rate at which pulses are transmitted
($f_r = \frac{1}{T}$)

During each interpulse period, T, the radar radiates energy for τ seconds and “listens” for target returns for the rest of the interpulse period. In general, the transmitted signal takes the form of a pulsed sine wave with an angular frequency

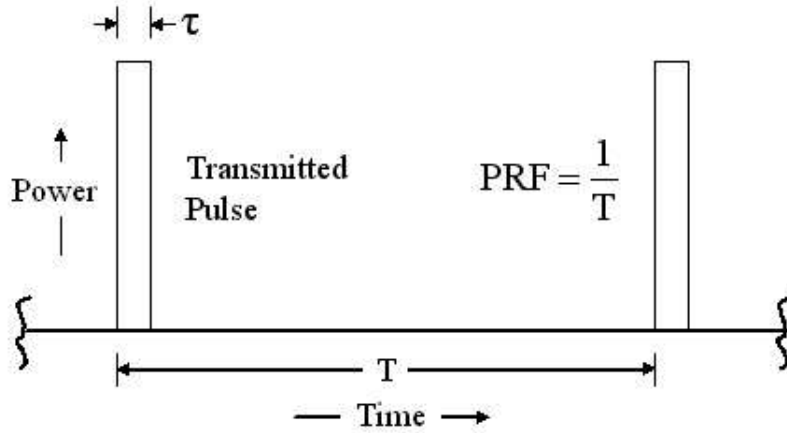


Figure 2.5 Illustration of Pulse Characteristics

ω_o , where ω_o is the carrier frequency or operating frequency. For long range military and air traffic control search operations, the frequency band utilized is between 1.0-2.0 GHz, classified as L-band.

The received energy returned from a target located at distance R will have a time delay given by

$$\Delta t = \frac{2R}{c} \quad (2.3)$$

where c is the speed of light. Assuming the reflected energy from a particular pulse is received within the interpulse period T , there will be no range ambiguity, and the maximum unambiguous range as a function of the interpulse period or pulse repetition frequency, f_r , is given by

$$R_{max} = \frac{cT}{2} = \frac{c}{2f_r} \quad (2.4)$$

As an example, consider the case shown in Figure 2.6. Echo 1 represents the radar return from a target at range $R_1 = c\Delta t/2$ due to pulse 1. Echo 2 could be interpreted as the return from the same target due to pulse 2, or it may be the return from a target further away at range R_2 due to pulse 1. The fact that echo 2 could be from either pulse indicates there is a range ambiguity associated with echo 2 [12].

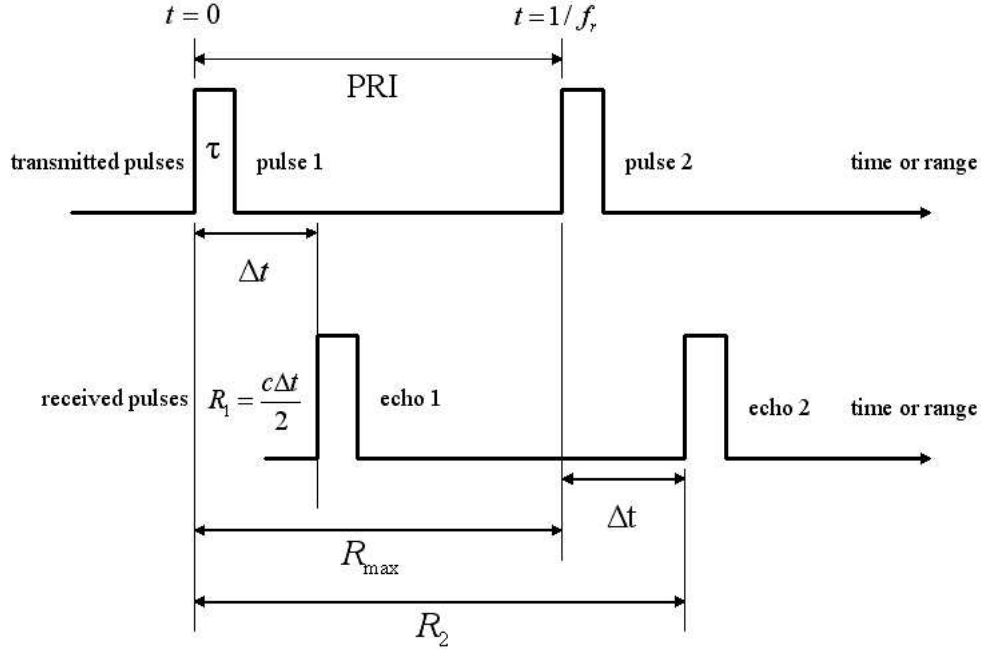


Figure 2.6 Range Ambiguity Illustration

2.3.2 Radar Equation. Following the development of [9], the radar equation is derived. The detection range of a radar system is primarily a function of three parameters: 1) transmitted power, 2) antenna gain, and 3) receiver sensitivity. An increase in transmit power will increase the radiated energy, which will result in a stronger return signal. If P is the power radiated by an antenna and power is radiated uniformly in all directions, the power per unit area or power density at a range R is given by

$$\text{Power density} = \frac{P}{4\pi R^2} \quad (2.5)$$

where $4\pi R^2$ represents the area of a sphere with radius R .

Most radars have a directive antenna that radiates power in a specific direction. This directivity is accounted for by incorporating the antenna gain into Eq. 2.5. The antenna gain at a particular angle, θ , is defined as the ratio of the radiated intensity at θ to the radiation intensity of a uniformly radiating antenna. The angle θ is illustrated in Figure 2.7 reproduced from [9]. At $\theta = 0$, the maximum gain of an

antenna is related to its physical area A and is given by

$$G = \frac{4\pi A \rho_a}{\lambda^2} \quad (2.6)$$

where A is the area, ρ_a is the antenna efficiency, and λ is the wavelength of the transmitted wave. Using this equation for antenna gain, the power density equation given in Eq. 2.5 is modified to provide the radiated power density of a directive antenna (P_{da}) as shown by

$$P_{da} = \frac{PG}{4\pi R^2} \quad (2.7)$$

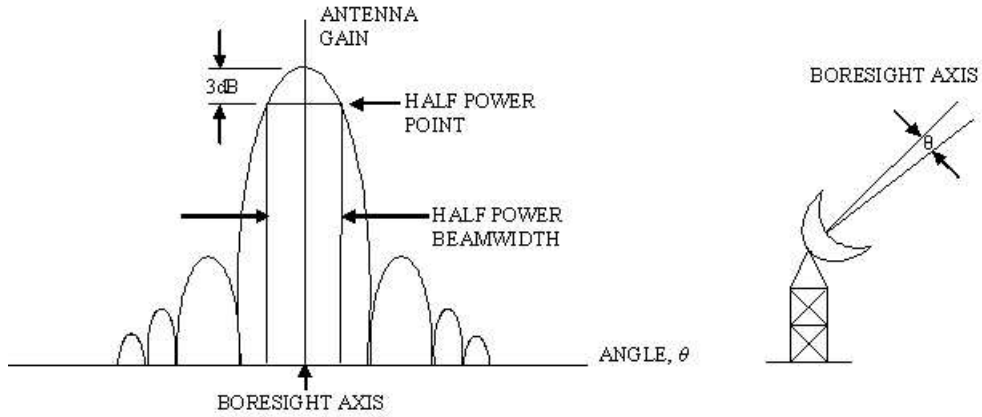


Figure 2.7 Antenna Gain Characteristics

When the radiated energy encounters a target, a portion of the energy is reflected back to the receiving antenna. The amount returned is dependent on the target scattering characteristics or the Radar Cross Section (RCS) denoted by σ , which has units of area (ft^2 , m^2). The RCS takes into account target size, orientation, physical shape, and material, and is normally measured experimentally [18]. Thus, the reflected power from the target becomes

$$\text{Reflected power from the target} = \frac{PG\sigma}{4\pi R^2} \quad (2.8)$$

Viewing the reflected power as a uniform source of power located at the target, the power density at the radar, a distance R away, can be calculated by

$$\text{Power density of reflected target power at the radar} = \frac{PG\sigma}{(4\pi R^2)^2} \quad (2.9)$$

At the radar, it is assumed the area capturing the energy is equal to the area of the receiving antenna, A . Assuming $\rho_a = 1$ for math simplicity, the power of the reflected signal at the radar is given by

$$\text{Power of reflected signal at the radar} = \frac{PG\sigma A}{(4\pi R^2)^2} \quad (2.10)$$

Solving Eq. 2.6 for A and substituting in Eq. 2.10 results in the power received (P_r) at the radar as shown in Eq. 2.11,

$$P_r = \frac{PG^2\lambda^2\sigma}{(4\pi)^3 R^4} \quad (2.11)$$

The target return power is only half of the story. In all practical applications, the returned signal received by the radar is corrupted with noise. This noise can originate within the receiver itself or it may enter the receiver through the receiving antenna. The M-code signal received by the antenna is one example of interference contributing to noise. One part of the noise generated within the receiver is due to the thermal agitation of electrons in the receiver. This thermal noise has the value given by

$$\text{Thermal noise} = kTB_n \quad (2.12)$$

where $k = 1.38 \times 10^{-23} \text{ joule/degree Kelvin}$ is Boltzmann's constant, T is the noise temperature in degrees Kelvin, and B_n is the noise bandwidth in Hz. As previously mentioned, thermal noise is only one part of the receiver noise. To account for all of the receiver noise, Eq. 2.12 is multiplied by a figure of merit called the noise figure,

F_n . This multiplication results in the total receiver noise power

$$N = F_n k T B_n \quad (2.13)$$

Using the noise power in Eq. 2.13 and denoting the target power received by the radar in Eq. 2.11 as S , the signal-to-noise ratio, S/N , forms the radar equation given as

$$\frac{S}{N} = \frac{P G^2 \lambda^2 \sigma}{(4\pi)^3 R^4 F_n k T B_n} \quad (2.14)$$

where S/N is generally expressed in decibels (dB).

Since the target return signal is always accompanied by noise, the receiver must distinguish the signal from the noise. This procedure is described in the next section.

2.3.3 Target Detection. The following discussion on target detection is adapted from [11]. All of the material presented may not be applicable to this research effort; however, the validity of this analysis will be addressed at the end of this section.

The purpose of the radar receiver is to process the signal and detect the existence of a target in the presence of noise, which includes the interference from the M-code signal for this effort. The process is accomplished by the detection circuit within a receiver. A block diagram of a simple detection circuit is shown in Figure 2.8 [11].

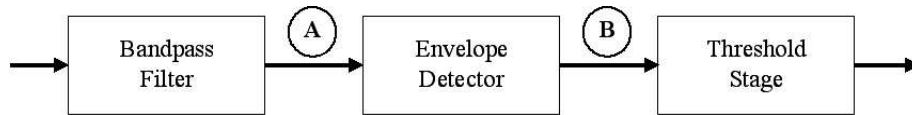


Figure 2.8 Simple Detection Circuit

The elements that make up the circuit include a bandpass filter, usually at the Intermediate Frequency (IF), an envelope detector, and a threshold circuit. The

threshold circuit compares the output of the envelope detector with a predetermined threshold. Whenever the envelope exceeds the threshold, a target is assumed to be present. This concept is illustrated in Figure 2.9.

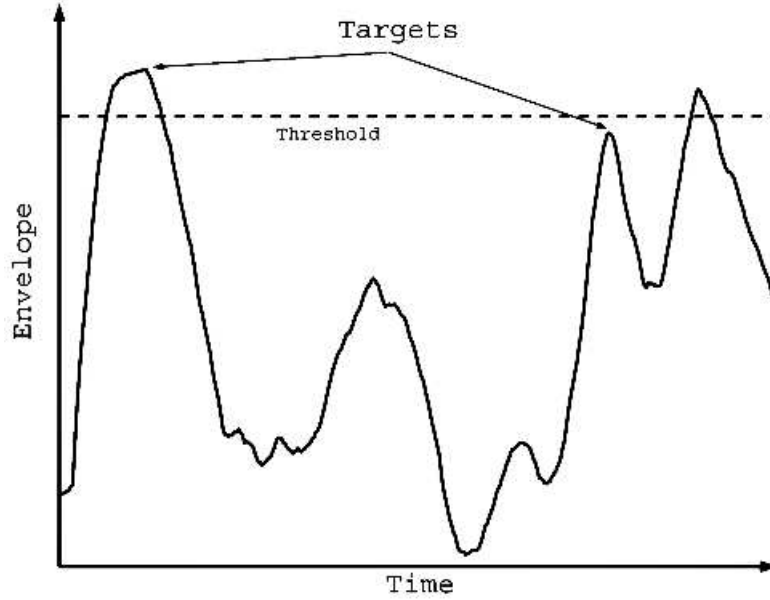


Figure 2.9 Detection Concept [11]

Figure 2.9 also shows one noise peak that would be mistaken for a target (the right-most peak). This threshold crossing is known as a false alarm. In addition, one target would not be detected because it is below the threshold, denoted a missed detection. A missed detection would indicate that the probability of detection (P_D) is less than one. Lowering the threshold would capture the missed target, thereby increasing the detection probability; however, it may also increase the false alarm probability (P_{FA}). One way to increase P_D without increasing P_{FA} would be to increase the signal so that the peak would be higher than the threshold, i.e., increase the signal-to-noise ratio, SNR.

To illustrate the discussion of P_D and P_{FA} , an analysis using the circuit of Figure 2.8 will be described for the detection of a single-pulse. Assuming the input consists of a sinusoidal signal with additive white Gaussian noise (AWGN), two probability density functions (PDF) of the envelope are required: a noise only case

and a case when both signal and noise are present. Using the PDFs and selecting a threshold value will determine the P_D and the P_{FA} .

Determination of these two joint PDFs requires first examining the noise. When white Gaussian noise is passed through a narrow bandpass filter, the output noise can be described by

$$n_o(t) = X(t)\cos(\omega_c t) + Y(t)\sin(\omega_c t) \quad (2.15)$$

where ω_c is the center frequency of the filter. $X(t)$ and $Y(t)$ are two independent random variables having a Gaussian PDF with zero mean and each having the same variance as $n_o(t)$. If the two-sided noise power spectral density (PSD) is $N_o/2$, and the bandpass filter has a rectangular response with bandwidth f_B , then the total average noise power, P_n , is determined by

$$P_n = \overline{X^2(t)} = \overline{Y^2(t)} = \overline{n_o^2(t)} = N_o f_B \quad (2.16)$$

where the bar over X , Y , and n_o indicate an expected value.

The signal, which is a sine wave of duration τ , and frequency ω_c , will pass through the filter virtually unchanged (assuming $f_B \gg 1/\tau$). At the bandpass filter output (point A in Figure 2.8), during the pulse length τ , the signal could be described by

$$s_o(t) = A \cos[\omega_c t - \phi_s] = a \cos(\omega_c t) + b \sin(\omega_c t) \quad (2.17)$$

where

$$A = (a^2 + b^2)^{1/2} \quad (2.18)$$

and

$$\phi_s = \arctan \frac{b}{a} \quad (2.19)$$

The combined signal plus noise at the output of the filter will be the sum of Eq. 2.15 and Eq. 2.17

$$\begin{aligned}
e_o(t) &= s_o(t) + n_o(t) \\
&= [a + X(t)]\cos(\omega_c t) + [b + Y(t)]\sin(\omega_c t) \\
&= r(t)\cos[\omega_c t + \phi(t)]
\end{aligned} \tag{2.20}$$

where

$$r(t) = \{[a + X(t)]^2 + [b + Y(t)]^2\}^{1/2} \tag{2.21}$$

and

$$\phi(t) = \arctan \frac{b + Y(t)}{a + X(t)} \tag{2.22}$$

Referring back to Figure 2.8, a linear envelope detector will yield, at its output (point B), the envelope $r(t)$, which can be rewritten as

$$r(t) = [X_1^2(t) + Y_1^2(t)]^{1/2} \tag{2.23}$$

where

$$X_1 = a + X(t), \quad Y_1 = b + Y(t) \tag{2.24}$$

Since both $X(t)$ and $Y(t)$ are independent zero-mean Gaussian random variables, X_1 and Y_1 are Gaussian random variables with means a and b respectively. Both are also independent and can be described by their corresponding PDFs shown in Eqs. 2.25 and 2.26.

$$p_1(X_1) = \frac{1}{\beta(2\pi)^{1/2}} \exp \left[\frac{-(X_1 - a)^2}{2\beta^2} \right] \tag{2.25}$$

$$p_2(Y_1) = \frac{1}{\beta(2\pi)^{1/2}} \exp \left[\frac{-(Y_1 - b)^2}{2\beta^2} \right] \tag{2.26}$$

Both X_1 and Y_1 have the same standard deviation β , which is equal to the root mean square (RMS) value of the noise $n_o(t)$ shown in Eq. 2.27.

$$\beta = [\overline{n_o^2(t)}]^{1/2} = (N_o f_B)^{1/2} \quad (2.27)$$

Since X_1 and Y_1 are independent, their two-dimensional joint PDF is equal to the product of Eqs. 2.25 and 2.26 and is given by

$$\begin{aligned} p(X_1, Y_1) &= p_1(X_1)p_2(Y_1) \\ &= \frac{1}{2\pi\beta^2} \exp \left[\frac{(X_1-a)^2 + (Y_1-b)^2}{2\beta^2} \right] \end{aligned} \quad (2.28)$$

Now a transformation to two other variables r and ϕ is made by using the relations

$$X_1 = r \cos \phi \quad Y_1 = r \sin \phi \quad (2.29)$$

or

$$r = (X_1^2 + Y_1^2)^{1/2}, \quad \phi = \arctan \frac{Y_1}{X_1} \quad (2.30)$$

The joint PDF of r and ϕ is obtained from the joint PDF of X_1 and Y_1 using the transformation

$$p(r, \phi) = \frac{p(X_1, Y_1)}{|J(X_1, Y_1)|} \quad (2.31)$$

where $J(X_1, Y_1)$ is the Jacobian of the transformation

$$J(X_1, Y_1) = \begin{vmatrix} \frac{\partial r}{\partial X_1} & \frac{\partial r}{\partial Y_1} \\ \frac{\partial \phi}{\partial X_1} & \frac{\partial \phi}{\partial Y_1} \end{vmatrix} = \begin{vmatrix} \frac{X_1}{r} & \frac{Y_1}{r} \\ -\frac{Y_1}{r^2} & \frac{X_1}{r^2} \end{vmatrix} = \frac{1}{r} \quad (2.32)$$

Substituting Eqs. 2.28, 2.29, and 2.32 into Eq. 2.31 yields

$$p(r, \phi) = \frac{r}{2\pi\beta^2} \exp \left[\frac{-(r^2 + a^2 + b^2 - 2ra \cos \phi - 2rb \sin \phi)}{2\beta^2} \right] \quad (2.33)$$

The PDF of the enveloper can be obtained by integrating $p(r, \phi)$ over all the phases

$$p(r) = \int_0^{2\pi} p(r, \phi) d\phi \quad (2.34)$$

which can be written as

$$p(r, \phi) = \frac{r}{2\pi\beta^2} \exp\left[-\frac{(r^2 + A^2)}{2\beta^2}\right] \int_0^{2\pi} \exp\left[\frac{rA}{\beta^2} \cos(\phi - \phi_s)\right] d\phi, \quad (2.35)$$

where A and ϕ_s are the amplitude and phase of the signal as defined in Eq. 2.17. The solution of the integral

$$\frac{1}{2\pi} \int_0^{2\pi} \exp\left[\frac{rA}{\beta^2} \cos(\phi - \phi_s)\right] d\phi \quad (2.36)$$

is known as the modified Bessel function of order zero, $I_0(x)$, which simplifies the PDF to

$$p(r) = \frac{r}{\beta^2} \exp\left[-\frac{(r^2 + A^2)}{2\beta^2}\right] I_0\left(\frac{rA}{\beta^2}\right) \quad (2.37)$$

The PDF in Eq. 2.37 is called *Rician*, named after S.O. Rice. In developing Eq. 2.37 there were no restrictions on the signal amplitude A . Therefore, assuming $A = 0$, i.e., no signal, will yield the PDF of the envelope of narrow-band noise. Given $I_0(0) = 1$ results in a PDF given as

$$p_0(r) = p(r)|_{A=0} = \frac{r}{\beta^2} \exp\left[-\frac{r^2}{2\beta^2}\right] \quad (2.38)$$

which is the Rayleigh PDF. Figure 2.10 shows the two pdf plots given by Eqs. 2.37 and 2.38. The signal plus noise pdf assumes a SNR of $A^2/(2\beta^2) = 8$. In addition, a threshold level V_T is shown to indicate that whenever $r > V_T$, the detection of a target is declared.

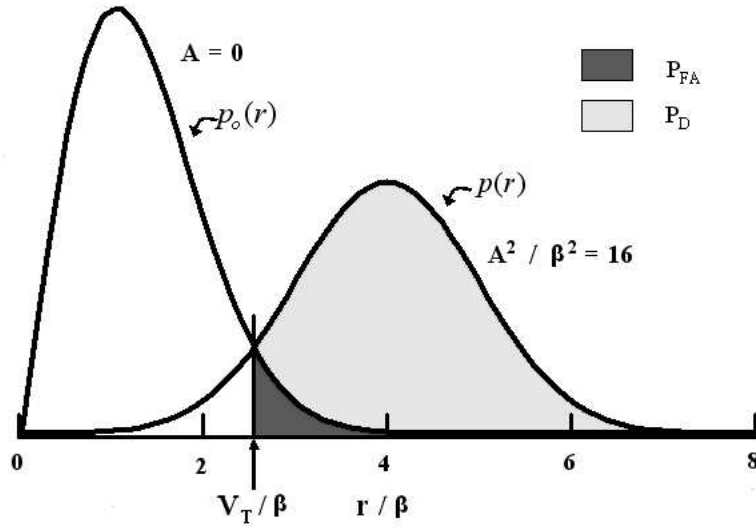


Figure 2.10 PDF of Detected Noise and Signal Plus Noise [11]

To determine P_{FA} , the area underneath $p_0(r)$ given by Eq. 2.38 needs to be evaluated from the threshold to infinity as shown in Eq. 2.39.

$$P_{FA} = \int_{V_T}^{\infty} \frac{r}{\beta^2} \exp \left[\frac{-r}{2\beta^2} \right] dr = \exp \left[\frac{-V_T^2}{2\beta^2} \right] \quad (2.39)$$

Similarly, to determine P_D , the area underneath $p(r)$ given by Eq. 2.37 needs to be evaluated from the threshold to infinity. However, the integral of Eq. 2.37 does not have a closed form solution and can only be expressed by tabulated functions. Yet, if the SNR is high, an approximation can be made. Given

$$SNR = \frac{S}{N} = \frac{A^2}{2\beta^2} \gg 1 \quad (2.40)$$

the PDF will have a sharp peak near $r = A$, which means the argument of the modified Bessel function, rA , can be replaced with A^2 . Using the approximation

$$I_0(x) \approx (2\pi x)^{-1/2} \exp(x), \quad 1 \ll x \quad (2.41)$$

yields, for large SNR,

$$p(r) \approx \frac{1}{(2\pi)^{1/2}\beta} \exp \left[\frac{-(r - A)^2}{2\beta^2} \right] \quad (2.42)$$

which is the Gaussian PDF. The integral of the Gaussian PDF is better known, yielding

$$P_D = P(V_T < r < \infty) \approx \frac{1}{2} \left[1 - \operatorname{erf} \left(\frac{V_T}{\beta\sqrt{2}} - (SNR)^{1/2} \right) \right] \quad (2.43)$$

where erf is the error function defined as

$$\operatorname{erf}(x) = \frac{2}{\sqrt{\pi}} \int_0^x e^{-t^2} dt \quad (2.44)$$

While the target detection process presented in this chapter utilizes an envelope detector, the simulation that will be presented in Chapter 3 employs a matched filter detection process. The information on the envelope detector was provided to show the general relationship between P_{FA} , P_D , and threshold selection, which will be applicable in the matched filter implementation.

2.4 Summary

In this chapter, the mathematical derivation of the M-code signal was presented. In addition, an overview of radars was provided, with an emphasis on detection, particularly how the probability of detection, probability of false alarm, and SNR interact. This working knowledge provides a conceptual basis for the simulation and results presented in Chapter 3.

III. Simulation Methodology, Results, and Analysis

3.1 Overview

This chapter presents the simulation methodology and the simulation results of M-code's effects on radar detection. A simulation description is presented first, listing the assumptions made for the simulation. Then the simulation process is described. The simulation and analysis are done in two phases: 1) the baseline case where the M-code is not present and 2) the interference case where the M-code (interferer) is present. The analysis uses detection probability (P_D) curves which show the detection probability versus input signal-to-noise ratio.

3.2 Simulation Description

As stated in Section 1.2, the overall objective of this thesis is to illustrate the effects the M-code signal has on radar systems. In particular, this simulation focuses on the effects the M-code signal has on a radar system's detection capability. The simulation is implemented in two phases. The first phase focuses on simulating the detection process in the presence of thermal noise only, without the presence of the M-code signal. The second phase adds the M-code signal as an interference source which the radar system must overcome in its detection process.

An important aspect of the simulation is that it is designed to look at a worst case radar detection scenario. As with any simulation, assumptions are made to facilitate the implementation. The assumptions made for this simulation are captured in Figure 3.1 and are summarized as follows:

1. *The return energy is from a stationary airborne point target.* Doppler and clutter effects are not considered.

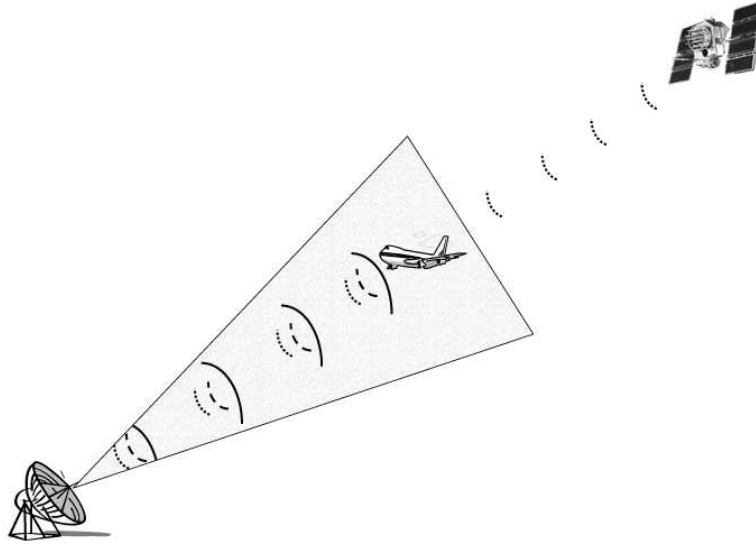


Figure 3.1 Simulation Scenario

2. *The simulation is done for a single pulse return.* This scenario is a worst case for detection, since benefits of pulse integration are not included.
3. *The RF GPS M-code signal is received in-line with the target return pulse.* Physically, this implies the target and transmitting GPS satellite are in direct line-of-sight with the radar (as shown in Figure 3.1). When aligned in such a manner, the received M-code signal has the maximum radar antenna gain applied to it (so it is worst-case).
4. *The radar carrier frequency is centered at one of the main lobes of the M-code signal (see Figure 3.2).* This location simulates a maximum received M-code signal power condition and again represents the worst-case scenario.
5. *Noise is modeled as additive white Gaussian noise (AWGN).*
6. *The detection threshold value is set using only AWGN with no interference present.*
7. *The M-code PN spreading sequence is assumed to be well modeled using a random binary sequence.* While the actual M-code is classified, this is a reasonable assumption.

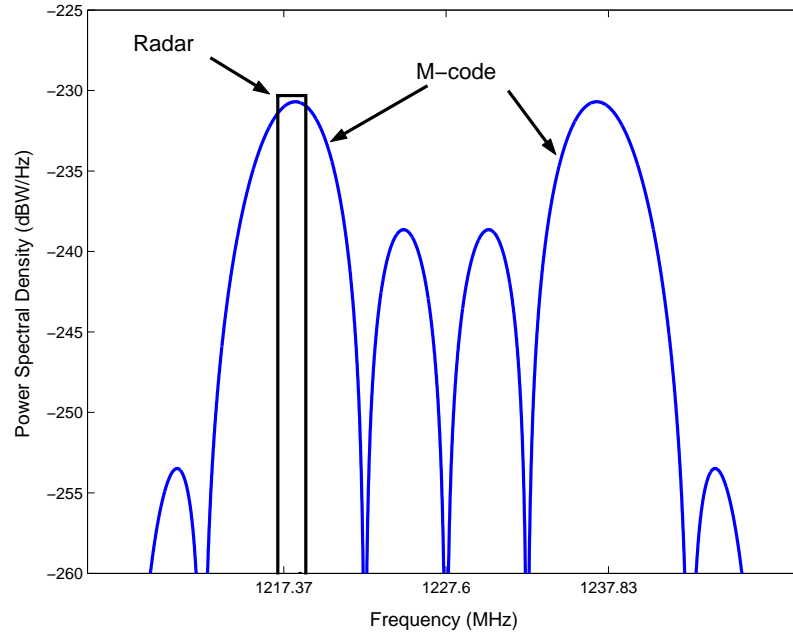


Figure 3.2 Radar RF Frequency Chosen to Maximize Received M-code Signal Power

The radar system model for this simulation is based on the Air Route Surveillance Radar Mode 4 (ARSR-4). The following discussion on the ARSR-4 system is taken from *Instruction Book, Field Maintenance, ARSR-4 System, Type FA-10331 Sections 1-10* [1].

The ARSR-4 system is a three-dimensional long range radar jointly used by the Federal Aviation Administration (FAA) and the United States Air Force (USAF). The system provides 360-degree azimuth coverage for ranges out to 250 nautical miles, at a height of up to 100,000 feet, and for elevation angles of -7 to +30 degrees.

The ARSR-4 radar is required to detect very small targets ($\sigma = 0.1 \text{ m}^2$ targets) at ranges up to 92 nmi and $\sigma = 2.2 \text{ m}^2$ targets at ranges up to 200 nmi. The radar has a range resolution of 1/16 nmi and a minimum range requirement of 5 nmi. To meet these requirements, the ARSR-4 radar transmits a wide pulse (150 μsecs) made up of two subpulses: one 90 μsecs wide and the other 60 μsecs wide. The two pulses

are transmitted at two different frequencies separated by 82.8572 MHz. The 60 μsec pulse, transmitted at the higher frequency, is narrow enough to meet the 5 nmi range requirement. The 90 μsec pulse, transmitted at the lower frequency, provides the additional energy needed to meet the larger range detection requirements. To meet the range resolution, the return echo is compressed to 0.772 μsecs which implies that each transmit subpulse is digitally phase-coded to create Non-linear Frequency Modulation (NLFM) with 1.3 MHz deviation. The radar transmits the 90 μsec pulse first, followed by the 60 μsec pulse. The operating parameters for the ARSR-4 system are summarized in Table 3.1.

Table 3.1 Operating Parameters for the ARSR-4 System

| Parameter | Value |
|-----------------------|---------------------------------|
| Peak Transmit Power | 63.765 kW |
| Average Power | 2.55 kW |
| Waveform Duty Cycle | 4.32 % |
| Antenna Transmit Gain | 37.7 dB |
| Antenna Receive Gain | 40.91 dB, max |
| Frequency | 1215-1400 MHz, duplex operation |
| PRF | 288 Hz |
| Scan Time | 12 secs |
| Azimuth Beamwidth | 1.4 degrees |

As previously stated, in this simulation the ARSR-4 system is simplified to be a single, uncompressed-pulse radar system, which is a worst-case approach. Use of the NLFM pulse compression should improve detection over the results shown in this research.

3.3 Simulation Process

Figure 3.3 illustrates the radar receiver model used for the simulations. The received signal (either signal plus noise or signal plus noise plus interference) is initially filtered by an RF Band Pass Filter (BPF_{RF}). The filtered signal then goes

through a two-step down-conversion process to take the signal from an RF-level down to an IF-level suitable for detection processing.

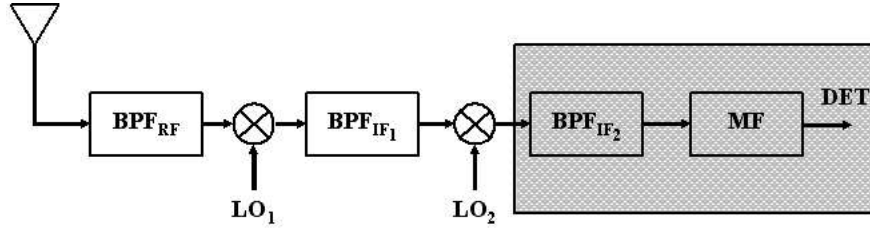


Figure 3.3 Receiver Model (Shaded Area Represents Portion Simulated in this Research)

Given the assumption the radar frequency is centered at a main lobe of the M-code signal, it is assumed the effects of the down-conversion process equally affect the returned radar pulse and the portion of the M-code signal received by the radar receiver. Thus, front-end filtering effects are neglected and the resulting SNR after the second local oscillator, LO_2 , is the variable simulation parameter. (If the radar frequency is not at a main lobe of the M-code signal, the M-code signal would have less impact than in the worst-case scenario that was simulated).

The remaining discussion on the simulation process focuses on the shaded region of Figure 3.3. The simulation is broken up into two cases—the baseline case (no M-code signal present), and the M-code case (with M-code present). Figure 3.4 presents a simulation flow diagram which describes the individual steps of the simulation. The shaded box represents the baseline case, while the rest of the diagram illustrates the steps that are followed for the interference case.

3.3.1 Baseline Case. The block diagram for the baseline case of the simulation is shown in Figure 3.5. The BPF_{IF} inputs are the return pulse, $s(t)$, and the noise term, $n(t)$. The return pulse is generated as a pulsed sinusoid at the IF frequency with duration τ , while the noise is zero-mean, additive white Gaussian noise (AWGN).

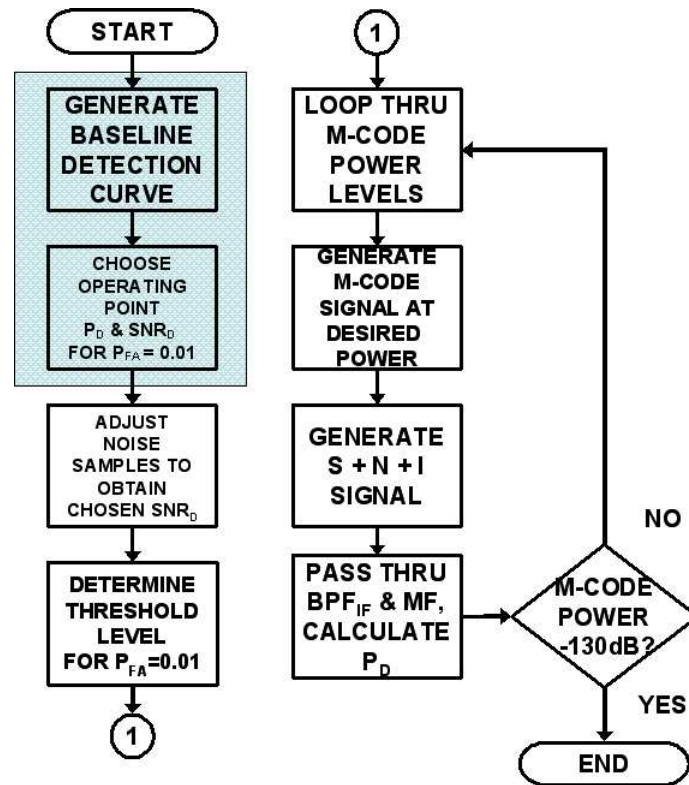


Figure 3.4 Simulation Flow Diagram to Determine the Effects of M-code on Radar Detection. Shaded Region Represents the Baseline Case.

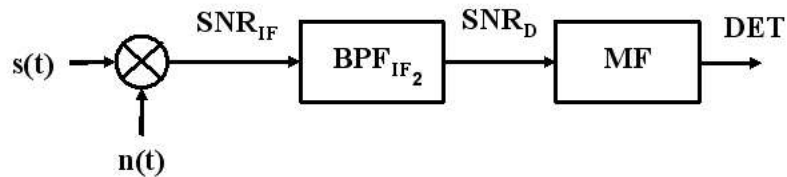


Figure 3.5 Baseline Simulation Block Diagram

The signal-to-noise ratio going into BPF_{IF} , SNR_{IF} , is determined by taking the ratio of signal power, P_s , and noise power, P_n calculated by

$$P_s = \frac{1}{N} \sum_{j=1}^N s^2(t_j) \quad (3.1)$$

$$P_n = \frac{1}{N} \sum_{j=1}^N n^2(t_j) \quad (3.2)$$

given a normalized 1Ω load. N is the number of samples in either the signal or the noise vectors. Since the simulation uses sampled data, the P_s and P_n calculated by Eqs. 3.1 and 3.2 represent average signal and noise power. In addition, in determining the noise power, a noise bandwidth given by $1/\Delta t$ is implied, where Δt is the time difference between two adjacent samples of the signal or noise vector. For this simulation, Δt is 1.25×10^{-7} secs, which gives an implied noise bandwidth of 8 MHz.

The BPF_{IF} bandwidth for this simulation was set to $1/\tau = 1/90 \mu\text{secs}$ or approximately 11 kHz, which is the 3.0 dB (or half-power) bandwidth. This value is typical for radar receivers of this type [9]. The filter selected for this simulation is an 8th-order Chebyshev bandpass filter with 0.1 dB bandpass ripple. The filter responses of the Chebyshev filter and an ideal filter are shown in Figure 3.6.

The BPF_{IF} filtering operation yields both filtered signal and noise components that are input into the matched filter. The matched filter is the heart of the detection process. The matched filter input SNR, SNR_{D} , is determined in the same manner used to determine SNR_{IF} , except the samples are now taken after the BPF_{IF} .

The matched filter is used to “match” the incoming signal with a known reference pulse. For this simulation, the original signal, $s(t)$, is modeled as the reference pulse. The matched filter can be implemented either as a correlation operation or a convolution operation. The latter is chosen for this effort. Convolution initially requires reversing either the incoming signal or the reference signal in time. The process involves convolving the incoming (filtered) signal with the reference signal

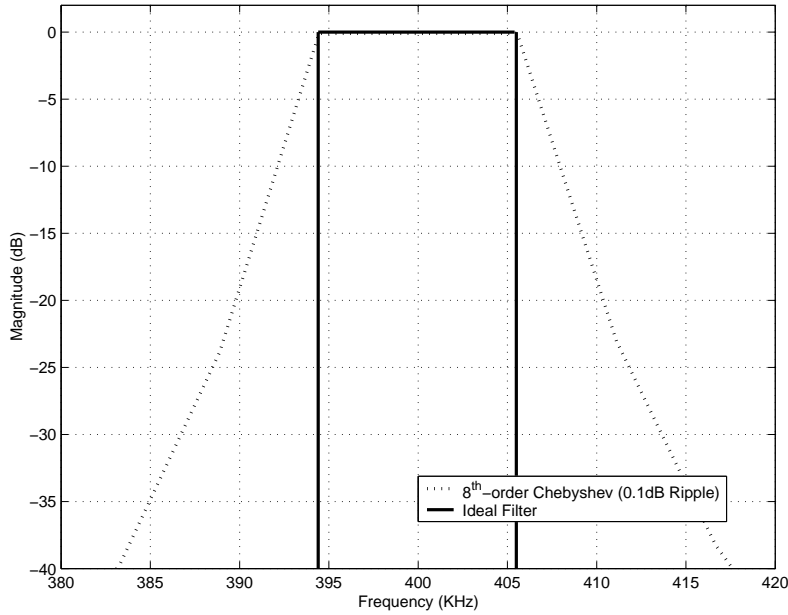


Figure 3.6 Filter Responses of an 8th-Order Chebyshev Filter and an Ideal Filter

by sliding the reference signal in time until the correlation is maximized. Since it is assumed the time delay of the return pulse is known and the return signal and reference signal sequences are the same length, the correlation is maximized when the two sequences completely overlap at time $t = \tau$, where τ is the pulse width. Thus, the maximum correlation will occur at the N^{th} sample out of the matched filter, since the signal and noise are both N samples long.

Since the N^{th} sample is the only value of concern (because the exact value of the return signal delay is assumed to be known), the time consuming convolution process was simplified for the simulation by an equivalent one-step process. The signal and noise were multiplied sample by sample and individual sample products were then added. The results of this multiplication and summation operation provides the same correlation value as the full convolution method described above.

The matched filter output is then compared to a threshold value to determine detection. Any value above the threshold indicates target detection, while a value below indicates no target present. As presented in Chapter 2, the probability of

detection (P_D) and the desired probability of false alarm rate (P_{FA}) depend on the threshold value. The desired threshold value is determined by fixing a value for P_{FA} and passing the noise samples through the matched filter. To be statistically perfect, an infinite number of noise realizations (N_{Real}) are required, which is not feasible. Therefore, the P_{FA} is used to determine the minimum number of simulated realizations needed to be statistically accurate, following the rule-of-thumb

$$N_{Real} \cong \frac{10}{P_{FA}} \quad (3.3)$$

The N^{th} sample for each noise realization passed through the matched filter is stored as a test statistic (Z), which is used in establishing a detection threshold. Once all the noise test statistics are collected, they are sorted and the threshold value is assigned to the $N_{Real} - (P_{FA} \times N_{Real})$ largest Z value. For example, for a $P_{FA} = 0.01$, 1000 noise realizations are required so that the 990th largest Z value is assigned as the threshold. This example is illustrated in Figure 3.7.

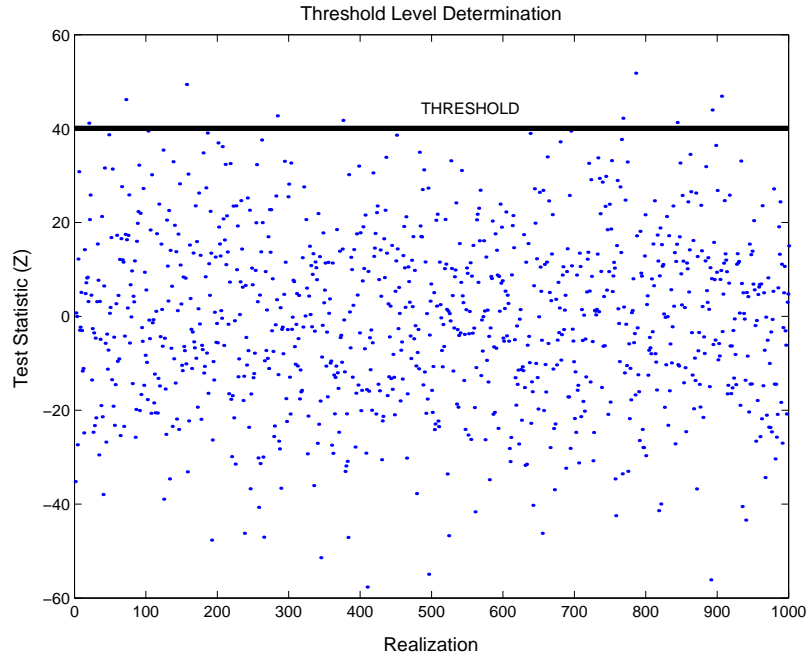


Figure 3.7 Threshold Determination Example

The matched filter processing is then repeated with a signal added to each noise realization to produce a new test statistic, Z' . The number of Z' values exceeding the pre-determined threshold value are counted and divided by the total number of Z values to estimate P_D . The estimated P_D is valid for a given P_{FA} and SNR_D . Therefore, to generate a complete detection picture (P_D versus SNR plot) requires the process be repeated over a range of desired SNR_D values, where each SNR_D produces a P_D for a constant P_{FA} .

Typically, radar applications require a P_{FA} on the order of 10^{-6} . However, due to computational resource limitations and time constraints, all subsequent research results (including the interference case) are based on $P_{FA} = 10^{-2}$.

Figure 3.8 shows a detection curve for the baseline simulation (no M-code present). The signal used to generate the curve is a pulsed sine wave of duration $\tau = 90 \mu\text{secs}$ at an IF frequency of 400 kHz, consistent with ARSR-4 specifications [1]. The noise is generated as zero-mean, AWGN with an unit magnitude average power. The value of SNR_D was changed by varying the pulse amplitude while keeping the noise power constant. The curve was generated by taking the noise samples and passing them through the 8th-order Chebyshev BPF_{IF} and the matched filter detection process to establish a detection threshold for a P_{FA} of 0.01. The signal amplitudes were then adjusted for varying SNR_D values, and the signal plus noise was then passed through the BPF_{IF} and matched filter to determine detection.

As Figure 3.4 indicates, operating points are selected from the baseline simulation to serve as the no interference reference points. From Figure 3.8, selecting a value for P_D fixes a value for SNR_D . Table 3.2 lists five operating points that will be used as part of the analysis in the next section.

The generation of Figure 3.8 and the selection of operating point parameters completes the baseline (i.e., no M-code interference) case. The next section presents

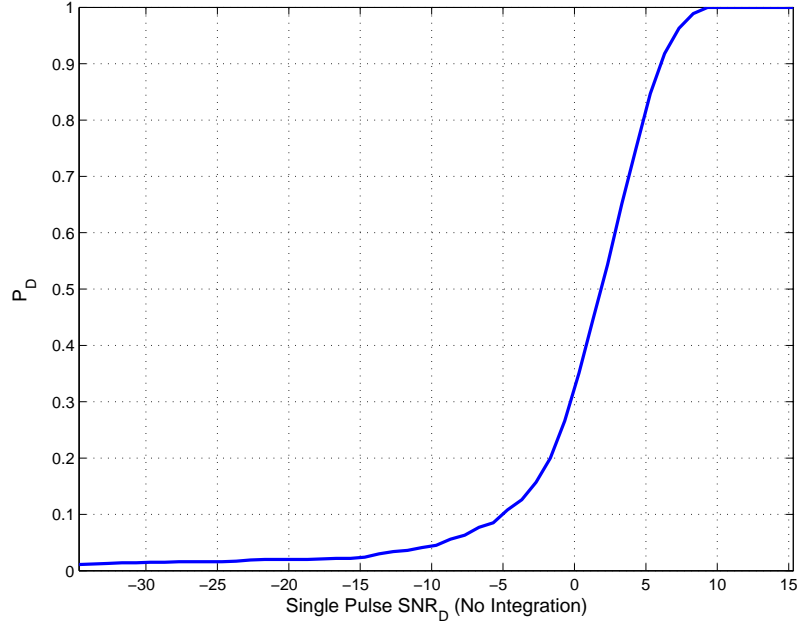


Figure 3.8 Probability of Detection Curve for a $P_{FA} = 0.01$

Table 3.2 Baseline Simulation Operating Points Used for Analysis

| P_D | SNR _D (dB) |
|-------|-----------------------|
| 0.9 | 6.06 |
| 0.8 | 4.83 |
| 0.7 | 3.81 |
| 0.6 | 2.84 |
| 0.5 | 1.86 |

the second phase of the simulation, which includes the modeling of a return pulse with the addition of M-code interference.

3.3.2 Signal Plus Noise Plus M-code Case. The block diagram for the second phase of the simulation is shown in Figure 3.9. The only difference between Figure 3.9 and Figure 3.5 is the addition of the M-code signal term, $M(t)$.

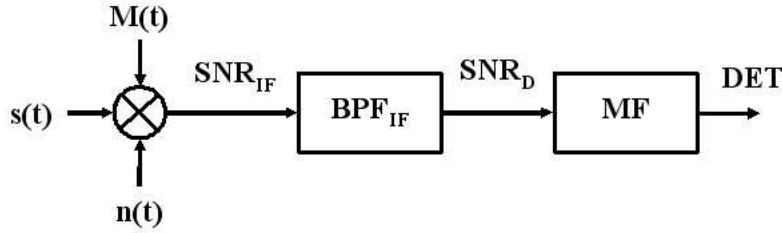


Figure 3.9 M-code Interference Simulation

In the baseline case, the noise power was kept constant while the return pulse amplitude was varied to obtain SNR_D . For the interference case, the return pulse power is kept constant and the noise samples are varied in magnitude to obtain the desired SNR_D value. The return pulse power is held constant because it is important to model the relative power levels between the radar and M-code signals correctly. This power relationship is maintained by calculating the radar return signal power and the M-code power at the receive antenna output. (All other operations occurring after that point are the same for both signals and will not significantly affect the relative power levels between the radar return and M-code signal).

The radar return power after the receive antenna is calculated by Eq. 2.11. For a target with a $\sigma = 2.2 \text{ m}^2$ cross-section at a detection range of 200 nmi, the received power was calculated with the parameters listed from Table 3.1 (using a carrier frequency of 1217.37 MHz) (see Figure 3.2). The target cross section value and the detection range are consistent with the ARSR-4 system operation [1]. Since 200 nmi is the maximum detection range, the return signal power is a minimum for a target located at this distance. It is assumed that the M-code signal will have the

most interfering affect when the return signal power is at a minimum. Thus, the received signal power after the antenna is calculated as follows

$$\begin{aligned}
P_r &= \frac{PG^2\lambda^2\sigma}{(4\pi)^3 R^4} \\
&= \frac{(63.765 \times 10^3 \text{W})(10^{\frac{37.7}{10}})(10^{\frac{40.91}{10}})\left(\frac{3 \times 10^8 \text{m/s}}{1217.37 \times 10^6 \text{Hz}}\right)^2 (2.2 \text{m}^2)}{(4\pi)^3 \left(200 \text{nmi} \cdot \frac{1852 \text{m}}{1 \text{nmi}}\right)^4} \\
&= 16.56 \times 10^{-15} \text{W} \quad (\approx -138 \text{ dBW})
\end{aligned}$$

for the target of interest. (Note that the G^2 term is the product of two gains, because there are different gains for the transmit and receive antennas.)

Since the return power is fixed, the noise sample amplitudes (power) are adjusted to provide the variable parameter SNR_{IF} . For every value of SNR_{IF} , the original unit-power noise samples are scaled by a gain factor given by

$$Gain \ Factor = \sqrt{\frac{P_r}{10^{\frac{\text{SNR}_{\text{IF}}}{10}}}} \quad (3.4)$$

The gain factor was derived by solving the basic SNR_{IF} equation given by Eq. 3.5 for P_n and taking the square root.

$$\text{SNR}_{\text{IF}} = 10 \log_{10} \left(\frac{P_s}{P_n} \right) \quad (3.5)$$

where P_s and P_r are equivalent terms.

By properly adjusting the noise samples for the given return pulse to the correct SNR_{IF} , the SNR_{D} value, after the signal plus noise is passed through the BPF_{IF} , will be correct as well. This scenario is illustrated in Figure 3.10 which shows the required SNR_{IF} needed to get a corresponding SNR_{D} for a given P_D .

Since the noise power has changed, a new detection threshold value is determined. The process to establish a new detection threshold is the same presented

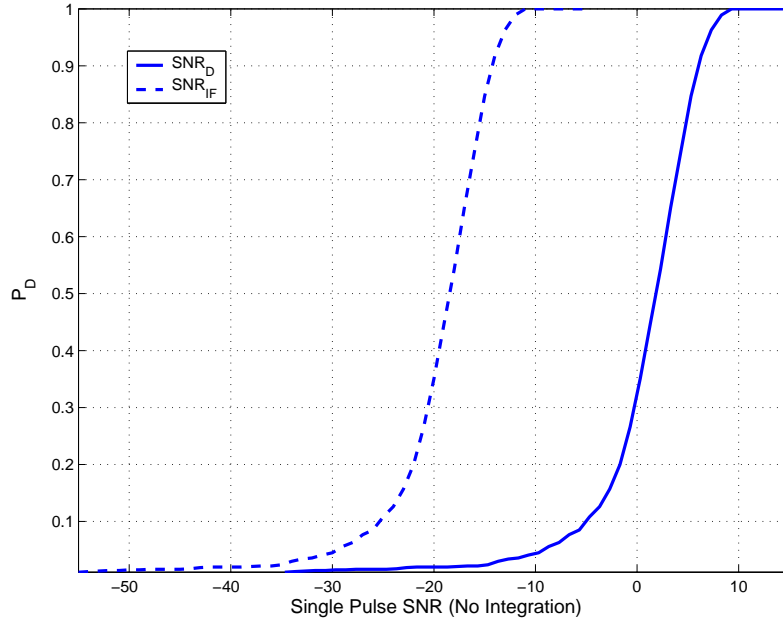


Figure 3.10 P_D versus $\text{SNR}_D/\text{SNR}_{IF}$ for $P_{FA} = 0.01$

for the first phase, except the noise in this case is the scaled, filtered noise signal. Once the return pulse signal and noise are correctly set, the M-code received power is varied to determine at what received power level the M-code begins to effect the established operating point P_D .

The M-code signal is generated using Eq. 2.1. As previously stated, the M-code PN sequence is assumed to be random and is generated as such. In addition, the M-code data stream, d_M , is assumed to be constant for the given signal duration. (This assumption is reasonable because the data bit interval is much longer than the return pulse duration τ .)

The generated baseband M-code sequence is used as the received M-code signal. The goal is to simulate a filtered $1/\tau$ bandwidth portion of the GPS M-code, where both the peak of the M-code signal and the filter are centered at IF (400 kHz). However, since the bandwidth of the M-code signal (24 MHz) is much wider than the center of the BPF_{IF} filter (400 kHz), a pre-filtering step is done to approximate the filter effects that would normally be in the front end of the radar receiver. This

operation eliminates frequency aliasing of the M-code signal about zero frequency that would occur if the signal was simply formed with the main lobe centered at 400 kHz. First, the baseband M-code sequence is generated at an IF frequency of 20.23MHz. The resulting IF signal is passed through a bandpass filter centered at 10MHz with a bandwidth of 500KHz to capture the lower main lobe of the M-code signal. Finally, the filtered M-code signal is down-converted to the center frequency of the IF filter located at 400KHz. It is assumed that this procedure is equivalent to most downconversion and filtering processes that are found in radar receiver front ends and will result in capturing the maximum M-code signal power as previously shown in Figure 3.2. Once the M-code signal is passed through the BPF_{IF} , it has the desired $1/\tau$ bandwidth.

Initially, the received M-code power is scaled by the maximum receive antenna gain given in Table 3.1, since the return pulse power was calculated using this gain. The scaled M-code signal (interferer) is then added to the return pulse signal and noise. All three are then passed through the BPF_{IF} and the matched filter detection process which produces the P_D of interest.

In accordance with proposed M-code power levels, the M-code signal was added at received power levels ranging from -160 dBW to -130 dBW, where the received power is considered to be the power incident on the antenna. Applying the maximum receive antenna gain of 40.91 dB, the M-code signal prior to the BPF_{IF} was scaled from -160 dBW and -130 dBW up to -119.09 dBW and -90.09 dBW, respectively.

Figure 3.11 shows several P_D curves at different M-code interference values for a single M-code signal. (The effects of varying the phase or PN code of the M-code signal will be described later). Note that the x-axis shows the signal-to-noise ratio (SNR_D) not the signal-to-noise-plus-interference ratio. The results indicate that there is a minimal effect on the detection probability for the minimum specified received M-code power of -160 dBW. However, as this particular M-code signal is increased to its maximum value of -131 dBW, a larger SNR_D is required to obtain the

same P_D . For a $P_D = 0.9$, the increase in required SNR_D going from an interfering signal power of -160 dBW to -130 dBW is about 7.44 dB. An alternative way to view the results is presented in Figure 3.12, which shows P_D as a function of received M-code power for the given operating points. Again, at a received M-code power of -160 dBW, there are minimal effects, while at the maximum specified M-code signal power, the P_D for all operating points dropped considerably.

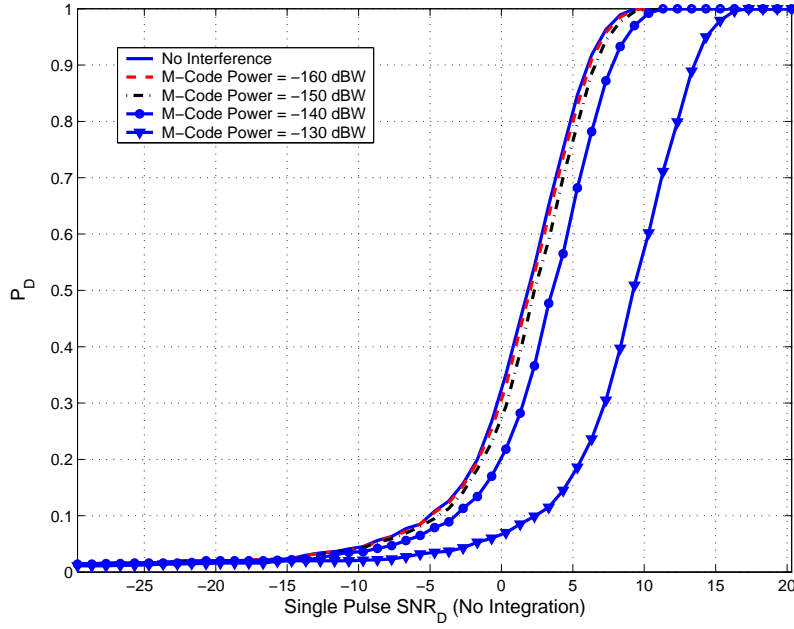


Figure 3.11 Detection Curves for Varying Levels of Received M-code Power for $P_{FA} = 0.01$

Since the radar was modeled as a single pulse system, the increase in required SNR_D for an increase in received M-code signal power seems appropriate. Most radar systems, including the ARSR-4, integrate over multiple pulses, which should (in theory) decrease SNR_D to produce the same P_D . Additional improvements can be obtained by a radar waveform providing orthogonality to the BPSK signal. Implementing NLFM will provide orthogonality and is a topic that will be revisited as a recommendation for further study.

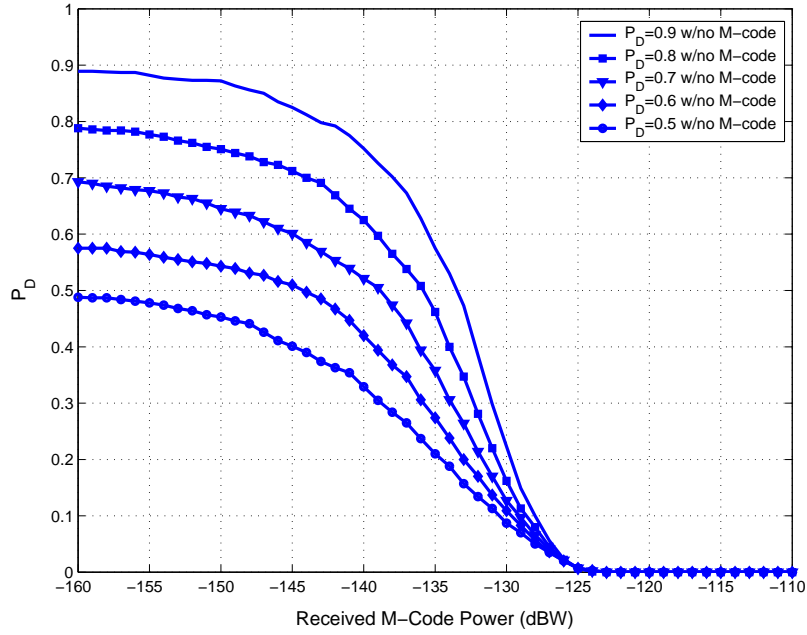


Figure 3.12 P_D vs Received M-code Power for $P_{FA} = 0.01$

Thus far, the results assumed the M-code was received perfectly in-phase with the radar return. Figures 3.13 - 3.16 illustrates the effects of phase offsets ranging from $-\pi$ to π in increments of 22.5° for received M-code powers of -160, -150, -140, and -130 dBW. Figure 3.17 shows the case for the specified -131 dBW power level. In all the figures, the dashed line is included as reference and represents the no interference detection curve. For received power of -160 dBW (Figure 3.13), changing phase offset values had little effect as all the curves are tightly bunched together. However, as the received power increases up to -130 dBW (Figure 3.16), the effects are dramatic. Depending on the phase offset, the curve shifts substantially, so much that at certain offsets, the P_D never increases above a nominal value.

The curves in Figures 3.11 and 3.12 were generated using the same randomly generated M-code sequence. When different sets of random sequences were applied, the curves shifted. Examples of the shift are illustrated in Figures 3.18 and 3.19 which show plots of 10 different M-code samples for received M-code power levels of -160 dBW and -131 dBW, respectively. Again, the dashed line is included as reference

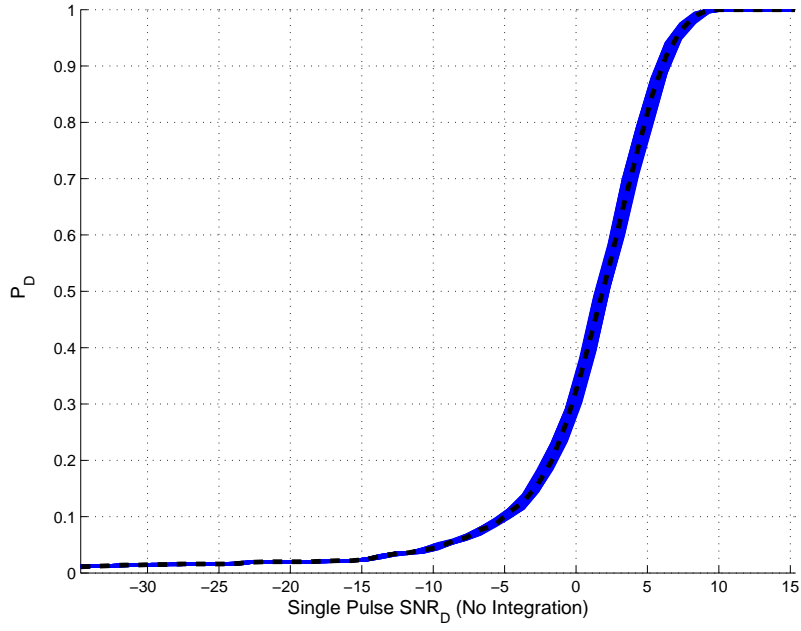


Figure 3.13 Effects of Phase Offsets on P_D for Received M-code Power of -160 dBW and $P_{FA} = 0.01$

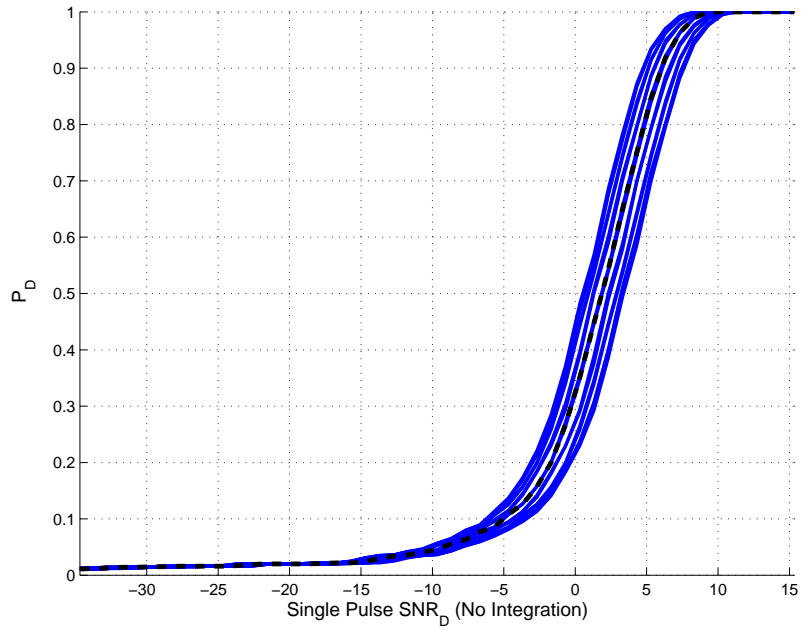


Figure 3.14 Effects of Phase Offsets on P_D for Received M-code Power of -150 dBW and $P_{FA} = 0.01$

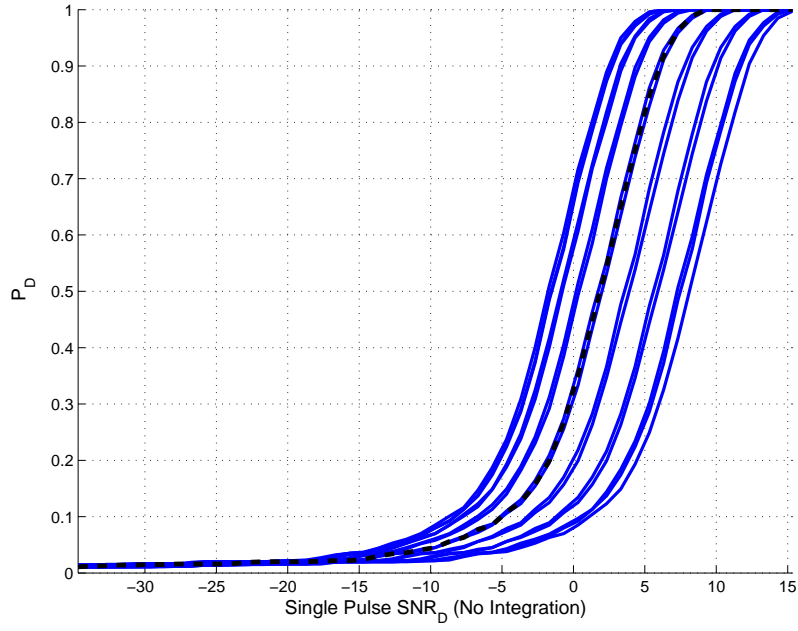


Figure 3.15 Effects of Phase Offsets on P_D for Received M-code Power of -140 dBW and $P_{FA} = 0.01$

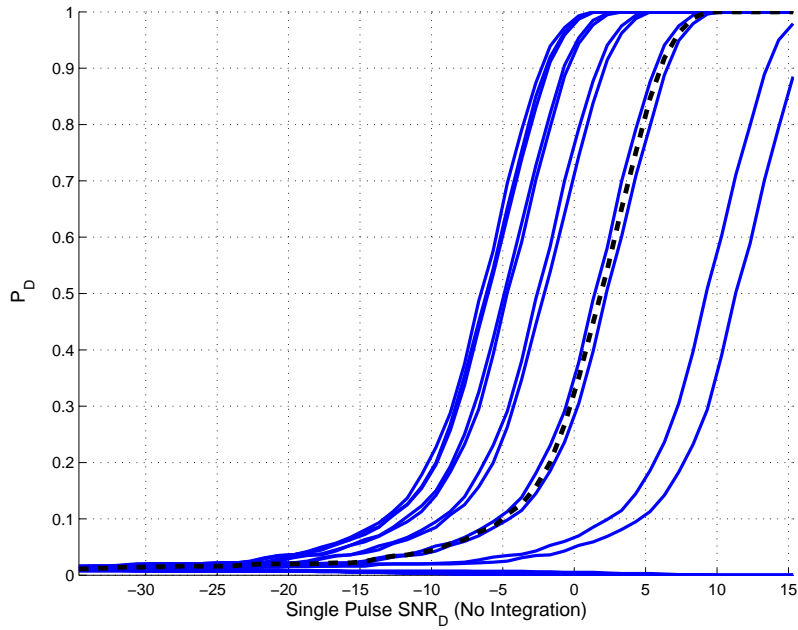


Figure 3.16 Effects of Phase Offsets on P_D for Received M-code Power of -130 dBW and $P_{FA} = 0.01$

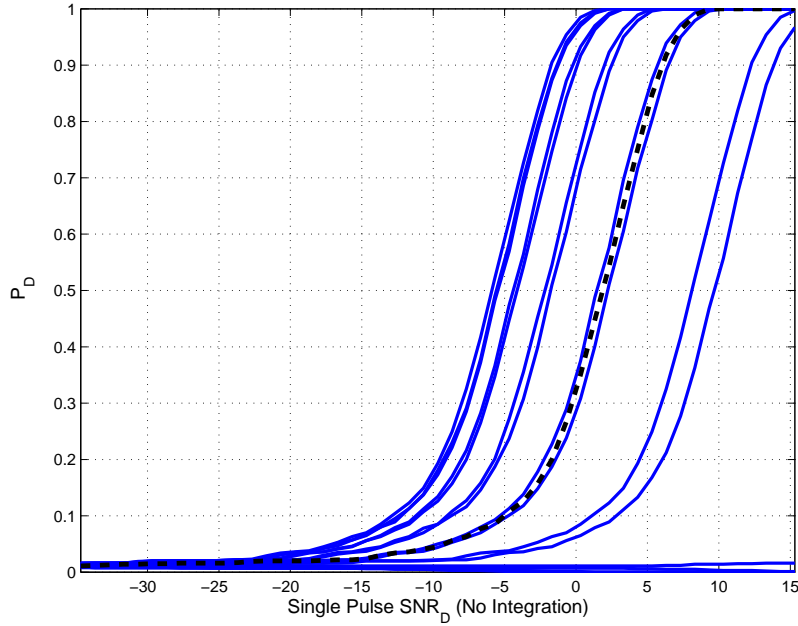


Figure 3.17 Effects of Phase Offsets on P_D for Maximum Specified Received M-code Power of -131 dBW and $P_{FA} = 0.01$

and represents the no interference detection curve. As observed with changing the phase offset, at the minimum received power level (Figure 3.18), the effects of using different M-code PN sequences were minimal. At the maximum received power level (Figure 3.19), the effects were severe. The difference in required SNR_D at $P_D = 0.8$ spanned 25 dB. Note that there are a total of 460 PN values over the 90 μsec pulse duration. Analyzing the sequences, 4 of the 10 had more +1 values than -1 values, but there was no correlation between this fact and the generated curves¹. Therefore, it seems that in addition to the phase, the M-code PN sequence over the 90 μsec pulse duration appears to be an important factor in determining the effects on detection at the maximum specified received M-code power.

For both the phase offset and random sequence results, the fact that the curves can shift either to the left or to the right would indicate the M-code signal can either add or subtract to the return signal, which is held constant. A curve shift to the

¹This is probably due to the fact that, because the signal is sampled, there is no guarantee that each +1 (or -1) M-code chip will increase or decrease the matched filter output by the same amount.

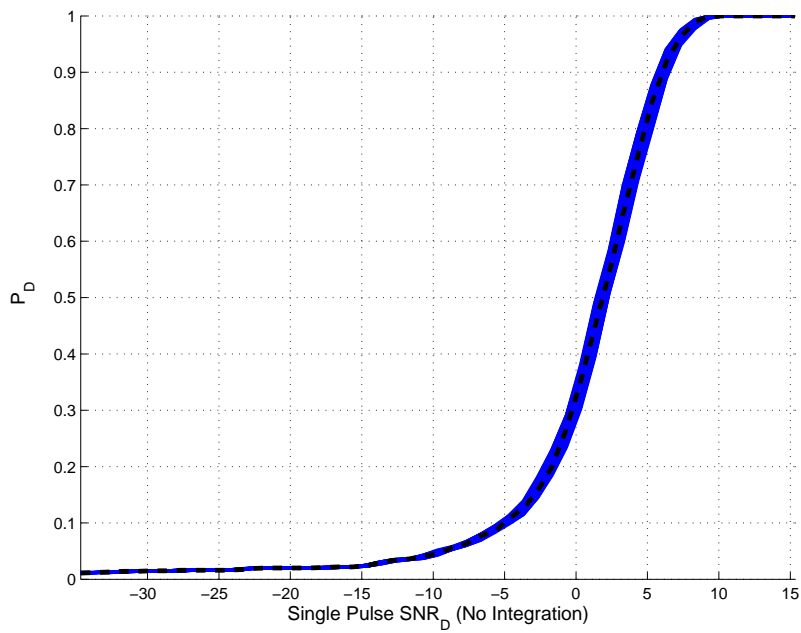


Figure 3.18 Comparison of P_D Curves Using Different Random M-code Sequences for Received M-code Power of -160 dBW

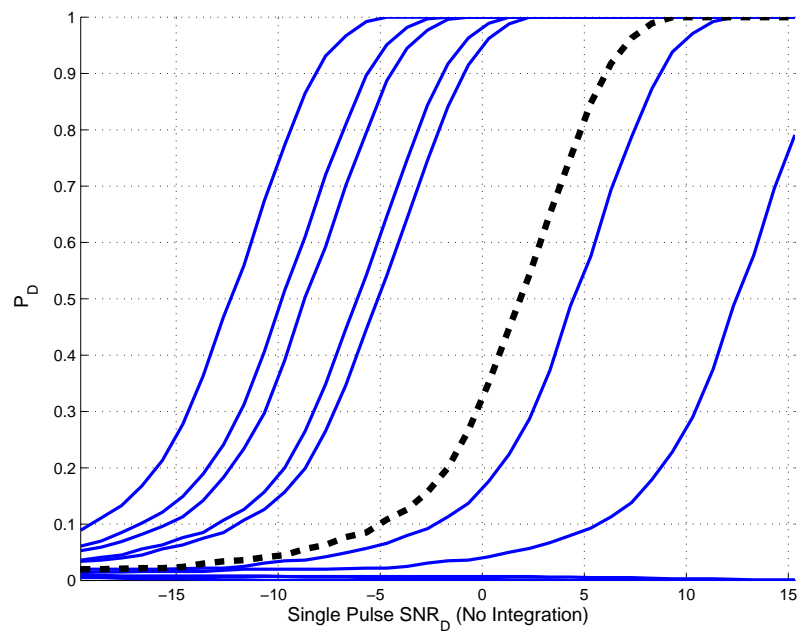


Figure 3.19 Comparison of P_D Curves Using Different Random M-code Sequences for Received M-code Power of -131 dBW

left indicates an increase in false alarms since the M-code signal is forcing more threshold crossings by effectively increasing the return signal samples (add effect). A curve shift to right, to the point where no detection is ever achieved, indicates the M-code signal is reducing the return signal samples so that the P_D is reduced (subtract effect). By changing the phase or using a different random sequence, the M-code signal had different effects (add or subtract) to the return signal on a sample by sample basis, which led to the results presented above.

3.4 *Summary*

In this chapter, the simulation methodology, simulation results and analysis to show the effects of the M-code on radar detection capability was presented. Two phases were discussed 1) a baseline case where only signal and noise were considered and 2) an interference case where the M-code signal was added. The results indicate for the minimum specified M-code power, the effects on detection are minimal. However, at the maximum specified M-code power, detection is greatly affected.

IV. Conclusion and Recommendations

4.1 Conclusion

This thesis presented the theory, simulation methodology, and results of simulating the detection process of a radar system and the effects the M-code signal has on that process. The simulation looked at a worst case scenario with the following key assumptions:

- The ARSR-4 was modeled as a single, uncompressed pulse radar system with no integration benefits.
- The return signal is from a stationary target located at the maximum target detection range. This scenario results in the lowest (worst-case) return power.
- The target and the GPS satellite broadcasting the M-code signal are in direct line-of-sight with the radar. The maximum radar antenna gain is applied to the M-code in this configuration.
- The detection threshold value is set using only AWGN with no interference present.

Additional assumptions were made and are listed in Section 3.2.

For a single pulse radar system, the results showed that M-code effects on the radar's detection capability were minimal when the received signal power was at the minimum specified value of -160 dBW. For the maximum specified M-code power of -131 dBW, the results indicate that the M-code signal will effect this radar system. The severity of the effects were shown to be dependent on the selection of the random M-code sequence as well as phase offsets. In the simulation, 10 different random sequences were applied and the results showed a difference in required SNR_D of approximately 25 dB for cases when a detection curve was generated. In three

cases, the P_D never increased above a nominal value. The effects of phase offsets had similar results. Note that these results only apply to a worst-case scenario for a single pulse as simulated for this research. Further modeling of the ARSR-4 radar system, to include use of NLFM pulse compression and pulse integration, would be necessary before definitively concluding that the M-code does or does not significantly affect radar system performance.

4.2 Recommendations

As stated, the worst case scenario assumed several things about the radar system and the M-code signal. Therefore, to augment this research effort, the following list of recommendations should be explored for a follow-on effort:

1. The simulation should be executed using a $P_{FA} = 10^{-6}$. As discussed, most systems, including the ARSR-4, require this P_{FA} . Due to time constraints, this research was performed using a $P_{FA} = 10^{-2}$.
2. Model the radar system as a NLFM pulse integrating radar detecting a moving target within a cluttered environment. As briefly mentioned in Chapter 3, providing orthogonality between the radar pulse and the M-code in the receiver, i.e. matched filter, will have a significant impact on the M-code interference rejection characteristics of the radar.
3. Obtain samples of the real M-code PN sequence, since the M-code PN sequence was generated as a random, binary sequence for the simulation. As the results indicated, the selection of the random sequence influenced how much effect the M-code had on the detection capability.
4. The assumptions made for the radar receiver front end needs to be further developed. The effects of the two-step downconversion were neglected and should be included.

5. Evaluate other radar systems operating in the L2 frequency band. Other systems will have operating parameters different than the ARSR-4 system.
6. Figure 3.7 showed an example of determining a threshold value where the test statistics were both positive and negative. Typically, test statistics should not be allowed to go negative. Therefore, the magnitude or squared magnitude of the test statistics should be employed.

Bibliography

1. *Instruction Book, Field Maintenance, ARSR-4 System, Type FA-10331, Sections 1-10*. Technical Instruction TI-6340.23, Baltimore MD: Westinghouse Electric Corporation, December 1999.
2. Anderson, Jon M. and David J. Lucia. "Analysis and Recommendation for the Reuse of the L1 and L2 GPS Spectrum." *Proceedings of ION GPS-98*. Alexandria VA: Institute of Navigation, 1998.
3. Anon. *Fact Sheet: U.S. Global Positioning System Policy*. Presidential Directive. Washington, D.C.: The White House, Office of Science and Technology Policy, National Security Council, 29 March 1996.
4. Barker, Brian C. and others. "Details of the GPS M Code Signal." *Proceedings of the Institute of Navigation, 2000 National Technical Meeting*. Alexandria VA: Institute of Navigation, 2000.
5. Betz, John W. "The Offset Carrier Modulation for GPS Modernization." *Proceedings of the Institute of Navigation, 1999 National Technical Meeting*. Alexandria VA: Institute of Navigation, 1999.
6. Betz, John W. "Analysis of M Code Interference with C/A Code Receivers." *Proceedings of ION 2000 National Technical Meeting*. Alexandria VA: Institute of Navigation, 2000.
7. Enge, Per and Pratap Misra. *Global Positioning System: Signals, Measurements, and Performance*. Lincoln MA: Ganga-Jamuna Press, 2001.
8. Holmes, J. K. and S. Raghavan. "GPS Signal Modernization Update Summary." *Proceedings of ION 58th Annual Meeting/CIGTF 21st Guidance Test Symposium*. Alexandria VA: Institute of Navigation, 2002.
9. Hovanessian, S.A. *Radar System Design and Analysis*. Norwood MA: Artech House, Inc., 1984.
10. Kaplan, Elliott D. *Understanding GPS, Principles and Applications*. Boston MA: Artech House Inc., 1996.
11. Levanon, Nadav. *Radar Principles*. New York NY: John Wiley and Sons, Inc., 1988.
12. Mahafza, Bassem R. *Radar Systems Analysis and Design Using Matlab*. Boca Raton FL: Chapman and Hall/CRC, 2000.
13. National Telecommunications and Information Administration. *U.S. Draft Proposal for WRC 2003*. Proposal. Washington D.C.: NTIA, 2002.

14. Navstar GPS Joint Program Office (JPO). *Navstar GPS Military-Unique Space Segment/User Segment Interfaces*. Interface Control Document. El Segundo CA: GPS JPO, 2001.
15. Pawlowitz, Timothy J. E-mail: timothy.j.pawlowitz@faa.gov. Federal Aviation Administration, 3 September 2002.
16. Pereira, R.C. Costa, Secretary General. Official Correspondence. ICAO, Montreal, Quebec, Canada, 10 August 2001.
17. Skolnik, Merrill I. *Introduction to Radar Systems* (Third Edition). New York, NY: McGraw Hill, 2001.
18. Stimson, George W. *Introduction to Airborne Radar* (Second Edition). Raleigh, NC: SciTech Publishing Inc., 1998.

| REPORT DOCUMENTATION PAGE | | | | Form Approved OMB No. 074-0188 | |
|--|-------------|--|-------------------------------|--|---|
| <p>The public reporting burden for this collection of information is estimated to average 1 hour per response, including the time for reviewing instructions, searching existing data sources, gathering and maintaining the data needed, and completing and reviewing the collection of information. Send comments regarding this burden estimate or any other aspect of the collection of information, including suggestions for reducing this burden to Department of Defense, Washington Headquarters Services, Directorate for Information Operations and Reports (0704-0188), 1215 Jefferson Davis Highway, Suite 1204, Arlington, VA 22202-4302. Respondents should be aware that notwithstanding any other provision of law, no person shall be subject to a penalty for failing to comply with a collection of information if it does not display a currently valid OMB control number.</p> <p>PLEASE DO NOT RETURN YOUR FORM TO THE ABOVE ADDRESS.</p> | | | | | |
| 1. REPORT DATE (DD-MM-YYYY) 25-03-2003 | | 2. REPORT TYPE Master's Thesis | | 3. DATES COVERED (From – To) Aug 2002 – Mar 2003 | |
| 4. TITLE AND SUBTITLE THE EFFECTS OF GPS M-CODE ON RADAR DETECTION | | | | 5a. CONTRACT NUMBER | |
| | | | | 5b. GRANT NUMBER | |
| | | | | 5c. PROGRAM ELEMENT NUMBER | |
| 6. AUTHOR(S) Yang, Jae, K., Captain, USAF | | | | 5d. PROJECT NUMBER If funded, enter ENR # | |
| | | | | 5e. TASK NUMBER | |
| | | | | 5f. WORK UNIT NUMBER | |
| 7. PERFORMING ORGANIZATION NAMES(S) AND ADDRESS(S) Air Force Institute of Technology Graduate School of Engineering and Management (AFIT/EN) 2950 Hobson Way, Building 640 WPAFB OH 45433-7765 | | | | 8. PERFORMING ORGANIZATION REPORT NUMBER AFIT/GE/ENG/03-20 | |
| 9. SPONSORING/MONITORING AGENCY NAME(S) AND ADDRESS(ES) SMC/CZE Attn: Lt. Bryan M. Titus 2435 Vela Way Suite 1613 El Segundo, CA 90245-5500 DSN: 833-6899 e-mail: Bryan.Titus@losangeles.af.mil | | | | 10. SPONSOR/MONITOR'S ACRONYM(S) | |
| | | | | 11. SPONSOR/MONITOR'S REPORT NUMBER(S) | |
| 12. DISTRIBUTION/AVAILABILITY STATEMENT APPROVED FOR PUBLIC RELEASE; DISTRIBUTION UNLIMITED. | | | | | |
| 13. SUPPLEMENTARY NOTES | | | | | |
| 14. ABSTRACT <p>The GPS system is undergoing a modernization effort which will add several new signals to be placed at the L1, L2, and L5 frequency bands. One of the signals to be placed on L2 is a new military code (M-code) which may be transmitted at a higher power level than current GPS signals. Other users of the L2 frequency band are concerned with the potential interference that may be caused by the increase in power of the GPS signal. One particular use of the 1215-1400 MHz frequency band is Air Traffic Control (ATC) radar applications.</p> <p>This thesis models the ARSR-4 radar system as a single pulse radar and simulates the effects that the M-code signal has on a radar system's detection capability. Looking at a worst case radar detection scenario, where the M-code signal power incident on the radar would be at a maximum, the results indicate that for the minimum specified received M-code signal power, the effects are minimal. However, for the maximum specified M-code signal power, the effects are quite noticeable to the point where the M-code may prevent detection of a single pulse.</p> <p>The results only apply to a worst-case scenario for a single pulse radar. Further modeling of the ARSR-4 system, to include pulse integration, would be necessary before a definitive conclusion can be drawn that the M-code will significantly affect radar system performance.</p> | | | | | |
| 15. SUBJECT TERMS Global Positioning System, GPS, Military Code, M-code, Modernization, Radar Detection, Radio Frequency Interference, RFI, Air Route Surveillance Radar Mode 4, ARSR-4 | | | | | |
| 16. SECURITY CLASSIFICATION OF: | | | 17. LIMITATION OF ABSTRACT | 18. NUMBER OF PAGES | 19a. NAME OF RESPONSIBLE PERSON |
| a. REPORT | b. ABSTRACT | c. THIS PAGE | | | John F. Raquet, Maj, USAF (ENG) |
| U | U | U | UU | 61 | 19b. TELEPHONE NUMBER (Include area code) (937) 255-3636, ext 4580; e-mail: John.Raquet@afit.edu |